Chemistry–A European Journal
Research Article
doi.org/10.1002/chem.202301212
Chemistry Europe
European Chemical Societies Publishing
www.chemeurj.org

Photo-Catalyzed α-Arylation of Enol Acetate Using Recyclable Silica-Supported Heteroleptic and Homoleptic Copper(I) Photosensitizers

Nathalie Body,[a] Robin Bevernaegie,[b] Corentin Lefebvre,[a] Ivan Jabin,[b] Sophie Hermans,*[a] Olivier Riant,*[a] and Ludovic Troian-Gautier*[a]

Earth-abundant photosensitizers are highly sought after for light-mediated applications, such as photoredox catalysis, depollution and energy conversion schemes. Homoleptic and heteroleptic copper(I) complexes are promising candidates in this field, as copper is abundant and the corresponding complexes are easily obtained in smooth conditions. However, some heteroleptic copper(I) complexes suffer from low (photo)stability that leads to the gradual formation of the corresponding homoleptic complex. Such degradation pathways are detrimental, especially when recyclability is desired. This study reports a novel approach for the heterogenization of homoleptic and heteroleptic Cu complexes on silica nanoparticles. In both cases, the photophysical properties upon surface immobilization were only slightly affected. Excited-state quenching with aryl diazonium derivatives occurred efficiently (10^8–10^{10} $M^{-1}s^{-1}$) with heterogeneous and homogeneous photosensitizers. Moderate but almost identical yields were obtained for the α-arylation of enol acetate using the homoleptic complex in homogeneous or heterogeneous conditions. Importantly, the silica-supported photocatalysts were recycled with moderate loss in photoactivity over multiple experiments. Transient absorption spectroscopy confirmed that excited-state electron transfer occurred from the homogeneous and heterogeneous homoleptic copper(I) complexes to aryl diazonium derivatives, generating the corresponding copper(II) center that persisted for several hundreds of microseconds, compatible with photoredox catalysis applications.

Introduction

Visible-light photoredox catalysis has emerged as an efficient tool to develop novel reaction pathways using mild and ecofriendly conditions. Despite being the most efficient organometallic photocatalysts, ruthenium(II) and iridium(III) complexes suffer from limitations in terms of sustainability and scalability. Alternatives based on organic and Earth-abundant photosensitizers, such as those based on iron, zinc or copper, have recently emerged.[1]

Homoleptic copper complexes $[Cu(NN)_2]^+$, where NN is a bidentate diimine ligand, were the first copper(I) complexes to be developed in photocatalysis. In the late 1980s, Kern and Sauvage reported the synthesis of $[Cu(dap)_2]^+$ (dap = 2,9-dianisyl-1,10-phenanthroline) and its application in the homocoupling of *p*-nitrobenzyl bromide.[2] Drawbacks such as the low excited-state lifetime of homoleptic complexes limited their applications, which led to their gradual disuse compared to Ru(II) and Ir(III) analogues.[1i] $[Cu(NN)_2]^+$ have nonetheless experienced a recent upsurge due to their notable reducing properties and the development of new diimine ligands enhancing the photophysical properties of such copper complexes.[1a,b,3] In an effort to improve the photophysical properties of these complexes, new derivatives of 1,10-phenanthroline ligands bearing bulky substituents were developed to prevent excited-state geometry changes *via* pseudo Jahn-Teller distortion.[4] In 2002, McMillin and coworkers drastically improved the field of copper photocatalysis by associating these sterically hindered diimine ligands with a diphosphine POP ligand (POP = bis[2-(diphenylphosphino)phenyl] ether). This led to the development of a new family of heteroleptic photocatalysts with excited-state lifetimes that can exceed those of ruthenium and iridium photocatalysts with blue-shifted absorbances.[5] Since then, heteroleptic copper complexes have been tremendously developed and their potential was demonstrated in multiple organic synthesis applications.[1i,o,6] However, it has been reported that heteroleptic copper complexes can sometimes suffer from ligand substitution and/or loss depending on the reaction conditions. This possible low (photo)stability leads to the formation of their homoleptic counterparts *via* a ligand association-dissociation mechanism that occurs more rapidly in coordinating solvents than in non-coordinating ones, for example.[7] This process can also occur upon oxidation of

[a] N. Body, Dr. C. Lefebvre, Prof. Dr. S. Hermans, Prof. Dr. O. Riant, Prof. Dr. L. Troian-Gautier
Université catholique de Louvain (UCLouvain)
Institut de la Matière Condensée et des Nanosciences (IMCN), Molecular Chemistry, Materials and Catalysis (MOST)
Place Louis Pasteur 1, bte L4.01.02, 1348 Louvain-la-Neuve (Belgium)
E-mail: sophie.hermans@uclouvain.be
olivier.riant@uclouvain.be
ludovic.troian@uclouvain.be

[b] Dr. R. Bevernaegie, Prof. Dr. I. Jabin
Université libre de Bruxelles (ULB)
Service de Chimie et PhysicoChimie Organiques (CPCO), Laboratoire de Chimie Organique (LCO)
Avenue F. D. Roosevelt 50, 1050 Bruxelles (Belgium)

Supporting information for this article is available on the WWW under https://doi.org/10.1002/chem.202301212

Cu(I) to Cu(II), either photochemically or electrochemically.[8] This association-dissociation mechanism also occurs in homoleptic complexes but the impact of such process is evidently less detrimental.[9]

Combining bulky ligands around the copper center is a solution to ensure a long-lived excited-state and a (photo)stable photocatalyst in solution, but it is not always sufficient to suppress that ligand exchange mechanism in coordinating solvents, as observed for [Cu(bcp)(DPEPhos)]PF_6 (bcp = bathocuproine, DPEPhos = bis[(2-diphenylphosphino)phenyl] ether) which forms the corresponding [Cu(bcp)$_2$]PF_6 complex under irradiation.[1p] Heterogenization on solid particles seems to be a promising approach to circumvent some of the above-mentioned limitations. Indeed, such an approach would restrict the degrees of freedom of the photosensitizers and potentially inhibit the association-dissociation mechanism. Moreover, we believe that developing approaches to recycle photosensitizers is paramount in the current energy and environmental landscape. Indeed, despite the low cost of heteroleptic copper(I) complexes such as [Cu(bcp)(DPEPhos)]PF_6 (2.5 times less expensive than $[Ru(bpy)_3]^{2+}$ (bpy = bipyridine) and 32 times less than [Ir(ppy)$_3$] (ppy = phenylpyridine)),[6f] developing versatile approaches to recover and isolate the metal is highly desirable to implement circular economy.[10] An added benefit in photoredox catalysis would also be the efficient separation of the heterogenized copper complexes that could be easily recovered by filtration from the reaction media.

Photocatalysts heterogenization has been studied as a powerful tool towards sustainable organic synthesis, amongst others.[11] Silica nanoparticles represent an optimal support as this inorganic oxide possesses i) a high specific surface area which can be tuned by the porosity parameters,[12] ii) an easy surface functionalization,[13] iii) a transparency over a broad range of wavelengths[14] and iv) a high mechanical and (photo)stability.[12] In organic photocatalysis, the heterogenization on silica supports has been developed mainly for organic dyes such as Rose Bengal,[15] Eosin Y[16] or BODIPY[17] as well as ruthenium(II)[18] and iridium(III) complexes.[19] To the best of our knowledge, there is only a handful of examples of well-defined copper complexes heterogenized on silica nanoparticles. For example, Cai and coworkers recently heterogenized a non-discreet copper complex $[Cu(NN)X_n]^+$ (X = I, Br, Cl, OAc or SO_4) on mesoporous silica nanoparticles for the thermal reactivity in organic synthesis.[20] Hosseinzadeh *et al.* anchored a phenanthroline-Cu(I) catalyst on nanocellulose which was used in thermal C–N and C–O cross-couplings reactions.[21]

The main photocatalytic domain for which copper complexes immobilization was developed is dye-sensitized solar cells (DSSC).[22] Numerous heteroleptic and homoleptic copper(I) complexes were immobilized on TiO_2 surfaces and revealed to be efficient for solar energy conversion.[1i] Efficient surface anchoring is achieved *via* the introduction of carboxyl[23] or phosphonate[24] groups on the chelating diimine ligand for example. The anchoring of heteroleptic copper(I) complexes was also applied for the photocatalytic hydrogen production by the Beller group.[25] Using sulfonated photosensitizers also anchored on TiO_2 composites along with $[Fe_3(CO)_{12}]$ as water reduction catalyst, a TON of 2452 could be reached in the photoproduction of H_2. For photocatalytic organic transformations, the immobilization of copper complexes has been rare. In 2020, Choi *et al.* developed a hybrid-copper catalyst anchored on SBA-15 (Santa Barbara Amorphous-15) silica nanoparticles.[26] By derivatizing the bipyridine ligand, a covalent bond was formed between the photoactive species and the support. This heterogenized system was then used in a photo-induced C–H arylation. Note however that no heteroleptic or homoleptic copper complex was involved, only a non-discreet complex. The only example of heteroleptic copper complex immobilization used in photocatalytic applications was described by Appleby *et al.* that used [Cu(xantphos)(dmp)](tfpb) (dmp = dimethylphenanthroline; tfpb = tetrakis(3,5-bis(trifluoromethyl)phenyl)borate) immobilized on chromatography grade silica by simple adsorption. These photoactive surfaces were then used to produce singlet oxygen upon irradiation with visible light in aqueous media to exterminate bacteria.[27] To the best of our knowledge, the immobilization of homoleptic or heteroleptic copper(I) complexes for photoredox applications is overlooked so far.

In here, we present an innovative approach for the heterogenization of heteroleptic and homoleptic Cu(I) complexes on silica nanoparticles and their use in the photocatalyzed α-arylation of enol acetate using aryl diazonium derivatives. Unambiguous heterogenization was confirmed by X-Ray Photoelectron spectroscopy (XPS), Transmission Electron Microscopy (TEM), Time of Flight Secondary Ion Mass Spectrometry (Tof-SIMS) as well as by Diffuse Reflectance UV-vis (DR-UV-vis). Comprehensive mechanistic details were garnered by steady-state and time-resolved spectroscopic techniques, which included transient absorption spectroscopy. The latter was used to determine that the heterogenized Cu(I) complexes were competent for excited-state electron transfer to the aryl diazonium derivatives with electron transfer rate constants that were in the 10^8–10^{10} $M^{-1}s^{-1}$ range. Importantly, the supported photocatalyst could be efficiently recovered and the photocatalytic activity only slowly decreased from 40 to 18% over 5 runs.

Results and Discussion

Synthesis

Siloxane moieties were considered to derivatize 1,10-phenanthroline-type ligands in order to achieve the final goal of immobilizing copper(I) complexes onto silica nanostructures. These anchoring moieties are suitable functions as they form strong anchor points with silica nanoparticles. In addition, the present study also investigates two different approaches to efficiently anchor copper(I) complexes, *i.e.* a one-step anchoring of well-defined homoleptic and heteroleptic copper(I) complexes and a two-step procedure where the heteroleptic complex was gradually assembled on the silica nanoparticles.

The targeted ligand functionalized with siloxane moieties (DMP-Si) was synthesized in three steps starting from the

commercial 2,9-dimethyl-1,10-phenanthroline (DMP) that underwent nitration in a mixture of concentrated sulfuric acid and fuming nitric acid to yield the corresponding 5-nitro-2,9-dimethyl-1,10-phenanthroline (DMP-NO_2). Subsequent reduction using hydrazine hydrate and carbon-supported palladium afforded the corresponding amine (DMP-NH_2). The last step was the formation of the ureido group through the reaction of DMP-NH_2 with triethoxy(3-isocyanatopropyl)silane to obtain the final DMP-Si ligand with an overall yield of 31 %. This ligand was then used for the synthesis of the corresponding homoleptic and heteroleptic copper complexes (Scheme 1). The homoleptic complex **(Cu-1)** was formed by dissolving the DMP-Si ligand in 2 : 1 ratio with $[Cu(MeCN)_4]PF_6$ in dichloromethane (DCM). For the heteroleptic complex **(Cu-2)**, DMP-Si was reacted in 1 : 1 ratio with a previously synthesized diphosphine copper complex ($[Cu(DPEPhos)_2]PF_6$) in DCM at room temperature for 3 hours. The homoleptic (**Cu-1**) and heteroleptic (**Cu-2**) complexes were obtained with isolated yields of 57 % and 61 %, respectively, and were characterized by Nuclear Magnetic Resonance (NMR), Differential Pulse Voltammetry (DPV) and Cyclic Voltammetry (CV), XPS, Fourier-Transform Infrared – Total Attenuated Reflectance (FTIR-ATR) and High Resolution Mass Spectrometry (HRMS) (see SI).

With the two complexes in hands, we sought to develop the synthesis of silica nanoparticles for efficient surface immobilization. Nanospheres (NS) nanoparticles were first targeted as they represent a standard morphology that prevents potential pore-diffusion issues, as commonly observed in heterogeneous catalysis.[28] Nanospheres nanoparticles were obtained by adapting the procedure of Stöber *et al.* based on the sol-gel process to access a 40 nm diameter size.[29] Core-shell (CS) silica nanoparticles were also targeted as this architecture offers a high specific surface area while limiting the diffusion of chemical species. Core-shell silica nanoparticles, with a core of 28 nm and a mesoporous layer of 16 nm, were obtained by adapting the procedure from Yoon *et al* also based on the sol-gel process.[30] The size and morphology of these NS and CS nanoparticles were confirmed by TEM (Figure 1). XPS (Figures S1 and S3) analysis showed that the 3D inorganic network of SiO_2 was correctly formed, and that no impurities were present, with the exception of NS for which a small

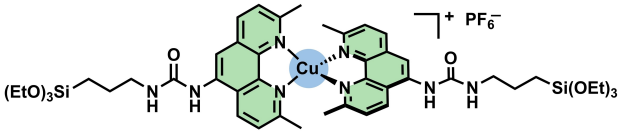

$[Cu(DMP\text{-}Si)_2]PF_6$ **(Cu-1)**

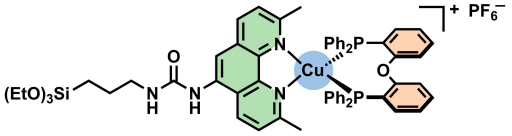

$[Cu(DMP\text{-}Si)(DPEPhos)]PF_6$ **(Cu-2)**

Scheme 1. Structures of the homo- and heteroleptic copper complexes **Cu-1** and **Cu-2**, respectively.

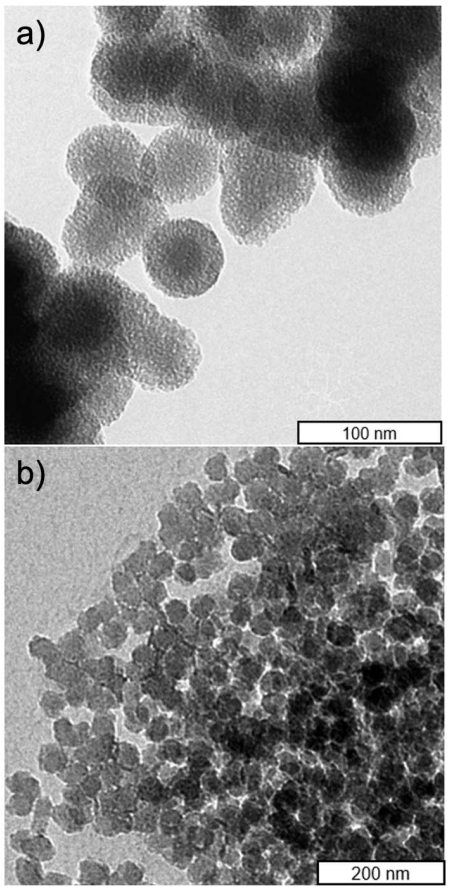

Figure 1. TEM images of pristine silica core-shell (CS) nanoparticles (a) and nanospheres (NS) (b).

amount of unreacted or partially reacted tetraethylorthosilicate (TEOS) was observed. Specific surface areas of 360 $m^2 g^{-1}$ and 650 $m^2 g^{-1}$ were calculated using the Brunauer-Emmett-Teller (BET) equation on nitrogen physisorption data for NS and CS, respectively (Figures S2 and S4).

First, the grafting of $[Cu(DMP\text{-}Si)_2]PF_6$ **Cu-1** was investigated on silica nanospheres. **Cu-1** was allowed to react with silanol functions of silica nanospheres in toluene under reflux over 24 hours (Scheme 2a). This afforded a deep orange-colored powder that was characterized by XPS and thermogravimetric analysis (TGA). All expected elements were detected at correct binding energies by XPS (Figure 2). The atomic ratios were in agreement with the one of pure **Cu-1** (Figure S5) corroborating that the complex's structure remained intact on the silica surface (Table 1).

Nevertheless, two unexpected components were observed for the F_{1s} signal by XPS, indicating that two types of fluorine environments were detected. The first one was attributed to PF_6^- appearing at a binding energy of 686.5 eV while the second one, with a binding energy of 688.3 eV, was attributed to F–(O,Si) bonds. The latter could come from an interaction between the counteranion and the support and explain the slightly decreased P/F atomic ratio obtained with XPS analyses. To bring that interaction into light, $[Cu(DPEPhos)_2]PF_6$ was stirred in DCM in the presence of pristine NS silica. After several

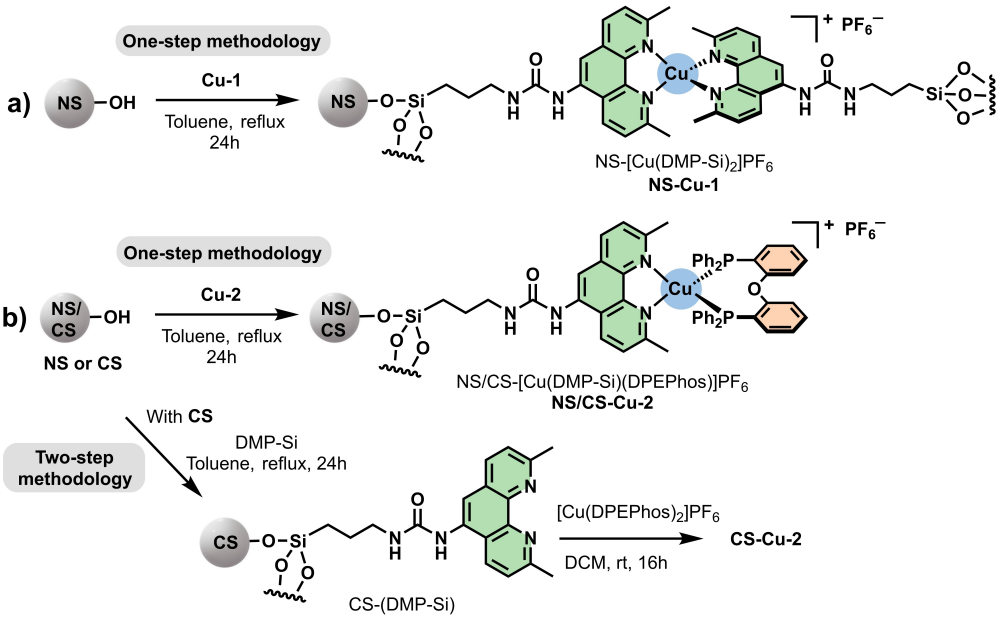

Scheme 2. The one- or two-step methodologies investigated to anchor the homoleptic (a) and heteroleptic (b) copper(I) complexes on nanospheres (NS) and core-shell (CS) silica nanoparticles. Note that both anchoring points of **NS-Cu-1** complex are probably located on the same silica nanosphere. **NS-Cu-2** was analyzed by ToF-SIMS and the corresponding color-coded fragments were detected, *i.e.* PF_6 (black, m/z = 145), Cu (blue, m/z = 63), Cu + DPEPhos (blue-orange, m/z = 602), Cu + DMP-Si (blue-green, m/z = 314) and Cu + DPEPhos + DMP-Si (orange-blue-green, m/z = 824). See Supporting Information for additional ToF-SIMS details.

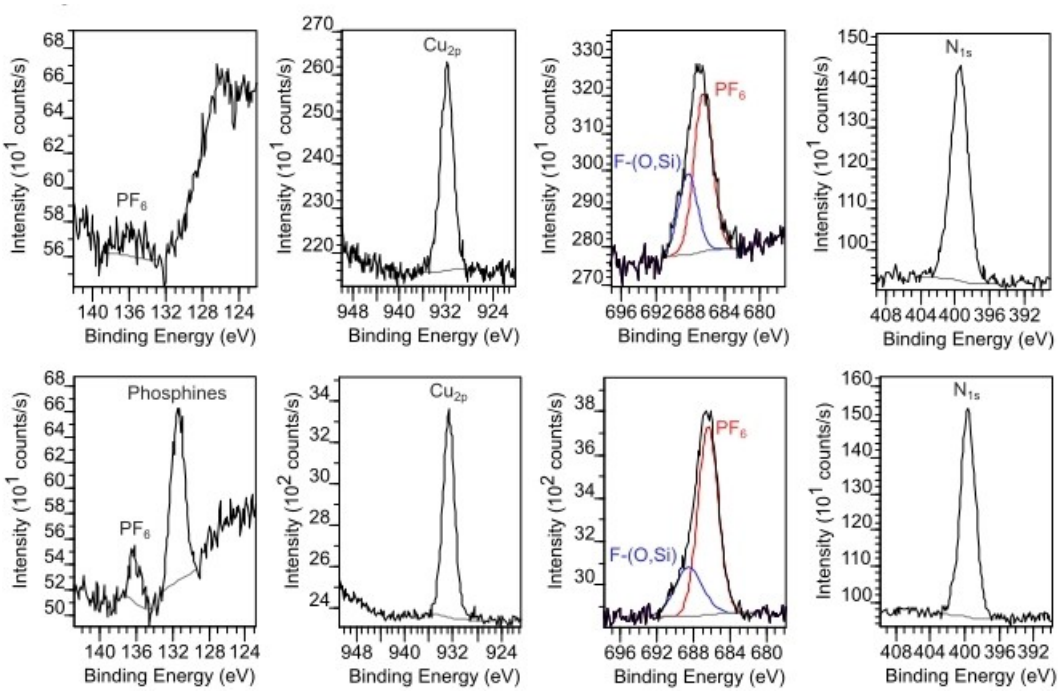

Figure 2. P_{2p}, Cu_{2p}, F_{1s} and N_{1s} XPS spectra of immobilized **NS-Cu-1** (top) and **NS-Cu-2** (bottom) obtained through the one-step methodology.

washing steps, the silica nanoparticles were analyzed by XPS where a fluorine signal was detected at 688.1 eV (Figure S28). This binding energy is in line with the one of O–F and Si–F bonds. As XPS is a semi-quantitative surface analysis, a TGA thermogram was recorded to quantify the loading of **Cu-1** at the surface of the support. The thermogram showed a loss in weight of about 15.6 wt.% which corresponds to 0.015 mmol of complex per 100 mg of material (Figure S17). This is consistent with standard loading values of copper comprised between 0.3–0.75 mmol g^{-1} found in the literature when considering the specific surface area ratios.[20a,c,31]

Table 1. XPS atomic ratios determined for the grafting of **Cu-1** and **Cu-2** onto CS or NS nanoparticles, in comparison with pure compounds. The theoretical ratio (in parenthesis) was calculated based on the molecular structures of **Cu-1** and **Cu-2**.

	Cu-1	NS-Cu-1	Cu-2	CS-Cu-2		NS-Cu-2
				Two steps[a]	One step[a]	One step[a]
N/Si	3.60 (4)	0.09	4.2 (4)	0.38	0.13	0.11
N/C	0.17 (0.17)	0.13	0.06 (0.07)	0.12	0.08	0.08
Cu/C	0.025 (0.021)	0.018	0.014 (0.017)	0.02	0.02	0.02
Cu/N	0.15 (0.125)	0.14	0.24 (0.25)	0.14	0.26	0.32
Cu/P	1.15 (1)	–	0.38 (0.5)[b]	0.89[b]	0.70[b]	1.40[b]
Cu/F	0.14 (0.17)	0.23	0.14 (0.17)	0.28	0.19	0.25
P/F[c]	0.12 (0.17)	–	0.15 (0.17)	0.07	0.08	0.04

[a] "One step" and "two steps" refer to the one- and two-step methodologies used for the preparation of the supported complexes (Scheme 2). [b] Only the phosphine component was used. [c] Only the phosphorus component arising from the counteranion was used.

Similar conditions were used to anchor the heteroleptic complex **Cu-2** on nanospheres and core-shell nanoparticles (Scheme 2b). XPS results were encouraging in both cases as all of the expected elements were detected at correct binding energies (Figure 2 and Figure S18) and all the atomic ratios were close to those of the pure copper complex (Table 1, Figure S9). The only mismatch came from Cu/P ratio that highlighted a slight deficiency of phosphine ligand and the P/F ratio, as described before, which was larger on NS than on CS nanoparticles. The loading was different from one support to the other, as expected based on the various specific surface areas. *Via* TGA, a loading of 0.014 mmol per 100 mg (wt.% = 14.8) and of 0.020 mmol per 100 mg (wt.% = 20.8) of material were determined for NS and CS, respectively (Figure S20). Inductively coupled plasma optical emission spectroscopy (ICP-OES) also corroborated the calculated loading obtained by TGA (wt.% in Cu = 0.82%, wt.% in **Cu-2** = 14.6%). As for the anchoring of **Cu-1**, these values are encouraging as the same range was found in the literature when considering the specific surface area ratios.[20a,c,31] Hence, this one-step anchoring procedure seemed efficient to preserve the copper complex's architecture. Smoother reaction conditions were also attempted with **Cu-2** (EtOH at room temperature instead of toluene at reflux) but only 0.03 at.% of Cu were detected by XPS (*vs* 0.7 at.% in toluene).

ToF-SIMS analysis was performed on **NS-Cu-2** to further confirm the efficient immobilization of complex **Cu-2**. In ToF-SIMS, surface sputtering with a focused primary ion beam generates the ejection of secondary ions that are easily collected and analyzed and provide molecular information. All the important fragments were detected by ToF-SIMS in negative (PF_6) and positive modes (Cu, Cu + DPEPhos, Cu + DMP-Si, Cu + DPEPhos + DMP-Si) (Scheme 2, Figure S19) which, in combination with the results obtained by XPS, unambiguously confirm the efficient immobilization of unaltered **Cu-2** at the surface of nanoparticles and highlights the efficiency of the proposed methodology.

In an effort to increase versatility of the silica support and expand the range of possible coordination reactions, a two-step methodology was also optimized where the ligand was anchored prior to being reacted with $[Cu(DPEPhos)_2]PF_6$ in dichloromethane at room temperature (Scheme 2b). The DMP-Si ligand was anchored onto CS by reacting the dense layer of silanols with the DMP-Si siloxane moieties. The formation of the CS supported ligand, *i.e.* CS-(DMP-Si), was confirmed by XPS analysis that showed a nitrogen peak at 399.4 eV corresponding to aromatic and urea nitrogen (Figure S23).[4] An experimental N/C atomic ratio of 0.19 was determined, which agreed well with the theoretical one of 0.22. In addition, TGA was also used to evaluate the ligand loading at the surface that showed a loss in weight of wt.% = 21.3, corresponding to a loading of 0.045 mmol of ligand per 100 mg of material, assuming that the calcinated organic part was only due to the presence of the DMP-Si ligand (Figure S24). With the efficient covalent immobilization of DMP-Si confirmed, we investigated the formation of the heteroleptic complex **Cu-2**. CS-(DMP-Si) was dispersed in DCM and a solution of $[Cu(DPEPhos)_2]PF_6$ in DCM was added dropwise. After an overnight reaction, a yellow powder was recovered and analyzed by XPS which confirmed the efficient formation of the immobilized heteroleptic complex **CS-Cu-2**, as emphasized by the presence of copper and diphosphine ligand peaks (Figure S25). Similar observations as in the anchoring of **Cu-1** were made for the F_{1s} signal indicating once again the interaction between the counteranion and the silica support. The atomic ratios were investigated to confirm that the expected structure was obtained (Table 1). Firstly, the N/Si ratio did not change compared to CS-(DMP-Si), confirming that the DMP-Si ligand was not altered or lost during reaction. The Cu/N was smaller than the theoretically predicted one, indicating that either some of the DMP-Si ligand was left unreacted, or that some homoleptic complex was also formed. This last hypothesis was reinforced by the lower than predicted percentage of phosphorus element. Finally, a loading of photoactive compound of 0.02 mmol of [Cu] per 100 mg of material was determined by TGA (Figure S26) which is slightly higher than the one obtained with the previously described methodology. Hence, the one-step methodology seems more suitable to preserve the structure of heteroleptic complex **Cu-2**.

Photophysical and electrochemical properties

The photophysical (Table 2) and electrochemical properties of $[Cu(DMP\text{-}Si)_2]PF_6$ (**Cu-1**) and $[Cu(DMP\text{-}Si)(DPEPhos)]PF_6$ (**Cu-2**) were first evaluated in homogeneous conditions. **Cu-2** absorbed moderately in the visible range with a maximum centered at 389 nm that tailed until 470 nm. A molar absorption coefficient around 2800 $M^{-1}cm^{-1}$ was determined at 389 nm which is in line with $[Cu(dmp)(DPEPhos)]BF_4$ ($\varepsilon = 2700\ M^{-1}cm^{-1}$ in DCM).[32] Visible light excitation of **Cu-2** led to steady-state photoluminescence (SSPL) centered at 560 nm. Time-resolved photoluminescence (TRPL) measurements in dichloromethane were well described by first-order kinetics which yielded excited-state lifetimes of 13.2 μs and 283 ns under argon and under O_2 saturated solution, respectively. **Cu-2** was also luminescent in acetonitrile with excited-state lifetimes of 2220 ns and 20 ns under argon and under O_2 saturated solution, respectively. Complex **Cu-1** exhibited a more intense and red-shifted absorption with a maximum centered at 464 nm with a corresponding molar absorption coefficient of 11000 $M^{-1}cm^{-1}$ in DCM which is in accordance with values for $[Cu(bcp)_2]PF_6$ ($\varepsilon = 13200\ M^{-1}cm^{-1}$ in DCM).[33] SSPL was observed at 704 nm in DCM under argon with a corresponding excited-state lifetime of 41 ns (Figure 3). The electrochemical properties of **Cu-1** and **Cu-2** were measured by cyclic and differential pulse voltammetry in MeCN containing 0.1 M $TBAPF_6$ electrolyte. For **Cu-2**, a metal-centered oxidation and ligand-centered reduction were recorded at 1.46 and −1.11 V *vs* NHE, respectively (Figures S10 and S11). Using the Rehm-Weller equation,[34] excited-state redox potentials $E_{1/2}(Cu^{+*/0}) = 1.09$ and $E_{1/2}(Cu^{2+*/+}) = -0.74$ V *vs* NHE were determined for **Cu-2**. These excited-state redox potentials are in line with the prototypical $[Cu(bcp)(DPEPhos)]PF_6$,[1p] highlighting that the introduction of a siloxane anchoring group did not change the fundamental properties of the complex. Concerning **Cu-1**, a metal-centered oxidation and ligand-centered reduction were recorded at 0.91 V and −1.12 V *vs* NHE (Figures S6 and S7), respectively, which yielded excited-state redox potentials of 0.64 V and −0.85 V *vs* NHE for $E_{1/2}(Cu^{+*/0})$ and $E_{1/2}(Cu^{2+*/+})$, respectively.

Table 2. Photophysical properties of **Cu-1** and **Cu-2** recorded in DCM.

Complex	Abs (nm)	PL (nm)	ε ($M^{-1}cm^{-1}$)	τ (ns)
Cu-1	464	704	11000	41 (Ar)
Cu-2	389	560	2830	13200 (Ar); 283 (O_2)

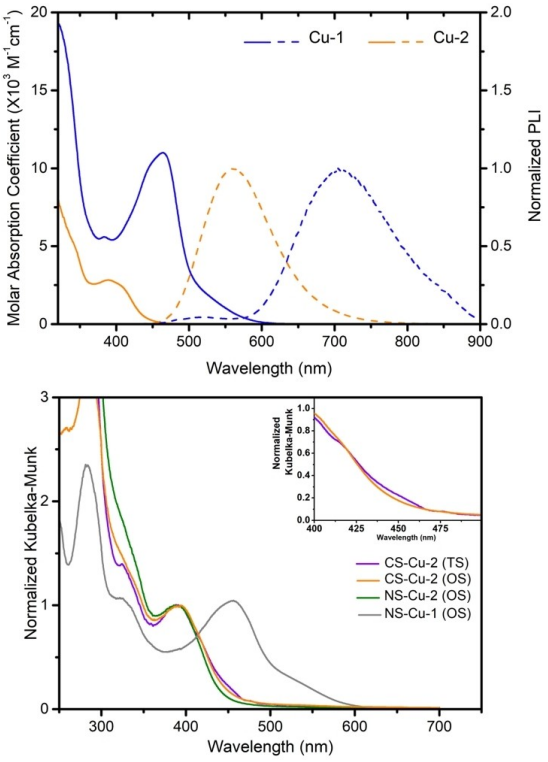

Figure 3. Top: UV-vis absorption (solid lines) and steady-state photoluminescence (dashed lines) spectra of **Cu-1** and **Cu-2** recorded in argon-purged DCM. Bottom: Diffuse reflectance spectra of **Cu-1** and **Cu-2** heterogenized on silica core-shell (CS) or nanosphere (NS) nanoparticles. OS = one-step methodology; TS = two-step methodology.

Similar photophysical properties were observed for the heterogenized copper complexes. The absorption profile was first assessed to confirm proper immobilization of the copper complexes without significant changes in their fundamental properties. To do so, diffuse reflectance UV-vis spectroscopy with a Kubelka-Munk treatment was performed. Anchored or not, the complexes showed the same absorption profile (Figure 3) and corresponding photoluminescence upon blue light excitation (Figure S27). Importantly, different diffuse reflectance spectra were obtained for **CS-Cu-2** whether the immobilization of the copper complex was performed in one or two steps. When a one-step immobilization approach was used, the diffuse reflectance spectra agreed well with the absorption spectra of **Cu-2** recorded in DCM. However, when the two-step procedure was used, a shoulder at 415 nm and a higher absorbance at 450 nm was observed which could potentially be attributed to the partial formation of **Cu-1**, albeit with the maxima slightly shifted compared to homogeneous conditions. This observation reinforces the previously proposed hypothesis that a portion of homoleptic complex was formed at the solid surface when a two-step methodology was used.

The SSPL spectra in DCM of **NS-Cu-2** functionalized nanoparticles were recorded following pulsed 410 nm light excitation. A very small shift of 6 nm was observed under argon atmosphere, with maxima centered at 561 and 555 nm in homogeneous and heterogeneous conditions, respectively. In the presence of oxygen, the PL intensity was almost completely quenched, indicating that this material is competent for $^1O_2$ photosensitization. In addition, this also highlights that, even if immobilized, the photoactive compound is still capable of undergoing excited-state reactivity. An excited-state lifetime of 3.8 μs was determined in heterogenous conditions, indicating that surface immobilization leads to additional excited-state deactivation processes.

We were then interested in investigating the stability of the heteroleptic complex in the dark and under irradiation. Indeed,

even if heteroleptic complexes represent a widely used class of photosensitizers for photoredox catalysis, their stability over the course of a reaction is not always investigated. It is also known that heteroleptic copper complexes can suffer from a lack of (photo)stability leading to the formation of their homoleptic counterparts *via* a ligand association-dissociation mechanism that occurs more rapidly in coordinating solvents than in non-coordinating ones for example.[7a,b,35] This is proper to heteroleptic copper(I) complexes but such light-induced degradation also occurs in prototypical Ru(II) photosensitizer where the dissociative ligand-field states can be easily populated.[36] In the dark or under irradiation, these heteroleptic Cu(I) complexes undergo ligand exchange to yield the corresponding homoleptic complexes which tend to be less effective in photoredox reactions. Strategies to mitigate these problems have been proposed over the years, the most famous one being the use of bulky substituents around the copper center.

In the present case, **Cu-2** did not undergo ligand exchange over 24 h in the dark in dimethylformamide, as evidenced by ^{1}H NMR (Figure S13). The photostability of this complex was then evaluated under 470 nm irradiation (Blue Thorlabs LED, Figure S31) in dimethylformamide, a suitable solvent for photoredox catalysis applications (*vide infra*). To do so, different concentrations of **Cu-2** were prepared and the absorption spectra were recorded at specific time intervals following irradiation with Blue Thorlabs LED. As can be observed from Figure 4, the presence of an isosbestic point at 420 nm coupled to the gradual increase of an absorption band at 475 nm is in line with the formation of the corresponding homoleptic complex **Cu-1**. Based on molar absorption coefficients, we estimated that 12% of **Cu-1** was formed after 4 hours of irradiation. In addition, it should be pointed out that this conversion was independent of the concentrations of photosensitizer and hence evolved according to a zero-order reaction. Similar experiments could not be performed on the heterogenized surfaces that require diffuse reflectance measurements, but those spectra were recorded following photoredox catalysis reactions (*vide infra*). Formation of the homoleptic complex **Cu-1** was also confirmed by ^{1}H NMR with similar conclusions as in the photostability study (55% of **Cu-1** formation after 24 h of irradiation) (Figure S14). Note that the changes of absorption features did not originate from the UV-vis spectrophotometer, as shown by control experiments (Figure S32). Photostability of **Cu-1** was also assessed using the same irradiation setup (Figure S31) which showed that **Cu-1** is photostable throughout 10 h of constant irradiation (Figure 4).

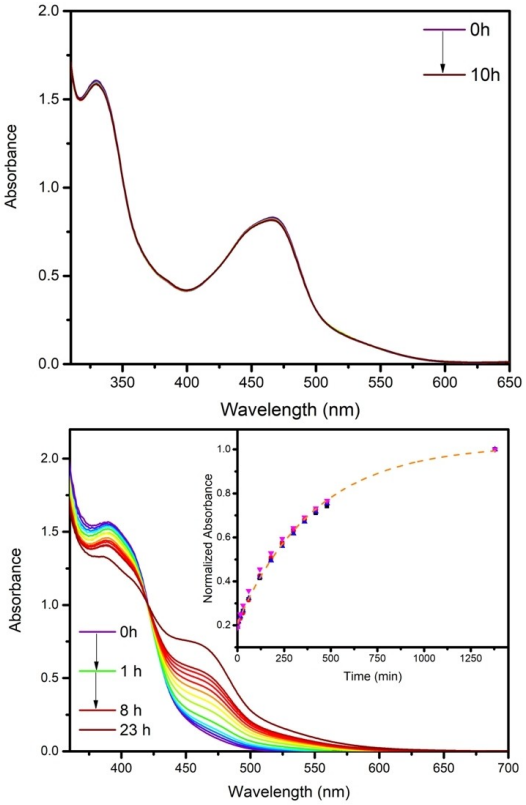

Figure 4. Photostability study of the homoleptic complex **Cu-1** (top) and of the heteroleptic complex **Cu-2** (bottom). Since degradation was observed for **Cu-2**, experiments were carried out at different concentrations (1.19×10^{-4} M = black square; 2.51×10^{-4} M = red circle; 3.47×10^{-4} M = blue triangle; 4.57×10^{-4} M = pink triangle) with the corresponding exponential fit (dashed orange line).

Excited-state reactivity

With a clear understanding of the ground and excited-states properties of the homogeneous and heterogenized copper complexes, we sought to investigate excited-state reactivity with an electron donor (*N*,*N*-diisopropylethylamine (DIPEA)) and an electron acceptor (4-nitrobenzene diazonium tetrafluoroborate). To do so, we performed excited-state quenching experiments following a Stern-Volmer approach. In homogeneous conditions using **Cu-2**, a quenching rate constant (k_q) of 4.1×10^7 $M^{-1}s^{-1}$ was determined with DIPEA in acetonitrile. This represents a very inefficient quenching process, and probably stems from the moderate driving force for electron transfer (−0.13 eV). When 4-nitrobenzene diazonium tetrafluoroborate was used, a much larger quenching rate constant of 2.3×10^9 $M^{-1}s^{-1}$ was determined in acetonitrile (Figure 5) along with a very favourable driving force for electron transfer (−1.14 eV). This value is very close to the solvent diffusion limit and highlights the efficiency for potential excited-state oxidative quenching. The Stern-Volmer experiments were more difficult to perform on **Cu-1** due to the short excited-state lifetime. No quenching rate constant could be determined with DIPEA or 4-nitrobenzene diazonium tetrafluoroborate in acetonitrile due to low emission intensity. These Stern-Volmer experiments were also conducted in dichloromethane on **Cu-2** and **Cu-1**. In both cases, the copper complexes were efficiently quenched by 4-nitrobenzene diazonium tetrafluoroborate with quenching rate constants of 1.2×10^9 $M^{-1}s^{-1}$ and 5.5×10^{10} $M^{-1}s^{-1}$ for **Cu-2** and **Cu-1**, respectively. No significant degradation was observed over the course of these experiments. Note however that some degradation was observed when steady-state photoluminescence quenching experiments were carried out in acetonitrile using **Cu-2** and 4-nitrobenzene

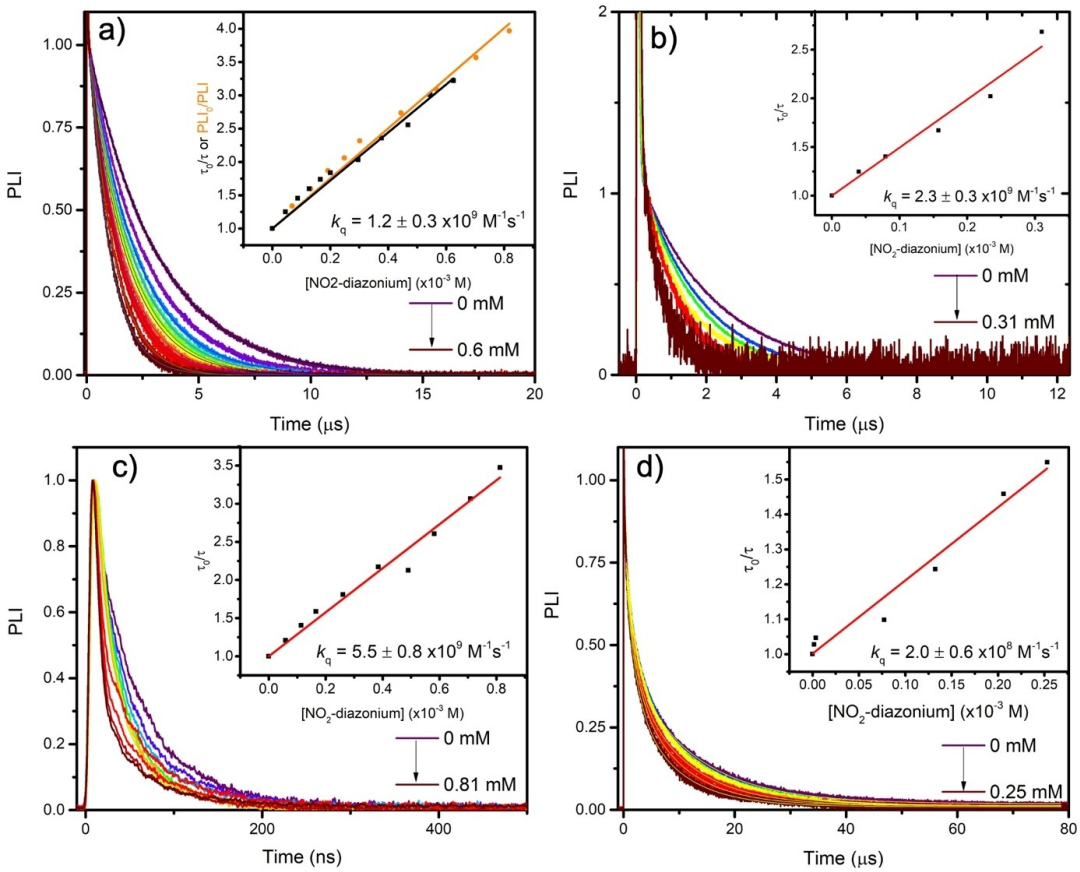

Figure 5. Excited-state quenching of **Cu-2** (a, b) and **Cu-1** (c) with increasing amounts of 4-nitrobenzene diazonium tetrafluoroborate in acetonitrile (b) and dichloromethane (a, c). Similar experiments were carried out with **NS-Cu-2** and 4-nitrobenzene diazonium tetrafluoroborate in dichloromethane (d). All experiments were carried out in argon purged solutions.

diazonium tetrafluoroborate (Figure S34). Steady-state photoluminescence quenching experiments were carried out in dichloromethane using **Cu-2** which yielded a quenching rate constant of 1.2×10^9 $M^{-1}s^{-1}$ (Figure S33).

To corroborate the photoredox catalysis experiments (*vide infra*), nanosecond transient absorption experiments were also conducted in DMF. Unfortunately, **Cu-2** did not exhibit sufficient photostability to obtain unambiguous transient absorption results. Indeed, when **Cu-2** was irradiated at 410 nm with ~10 mJ/pulse laser fluence, a positive signal gradually appeared at wavelengths consistent with the formation of the homoleptic complex. However, **Cu-1** was particularly well-suited for these transient absorption measurements. The photosensitizer was short lived in DMF, as in acetonitrile, which prevented us from rigorously characterizing the excited-state absorption spectra. We thus opted for an alternative solution and recorded the transient absorption spectra 200 ns after 470 nm pulse-light excitation. This led to no significant absorption changes, as expected, and was only used to set the baseline for these experiments and to confirm that no side reaction occurred with DMF on that timescale (Figure 6), unlike **Cu-2**. Identical measurements were performed in the presence of 10 mM of 4-nitrobenzene diazonium tetrafluoroborate. In that case, an intense negative signal was observed around 490 nm, consis-

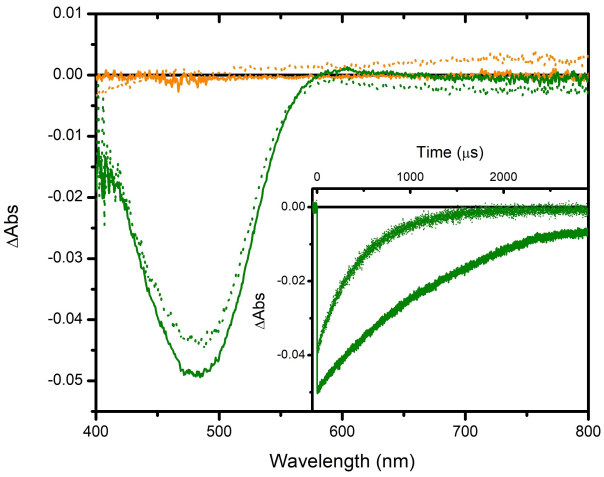

Figure 6. Nanosecond transient absorption spectroscopy recorded in DMF 200 ns after pulsed 470 nm light excitation of **Cu-1** (solid) and **NS-Cu-1** (dashed) without (orange) and with (green) 10 mM of 4-nitrobenzene diazonium tetrafluoroborate. The inset represents the single wavelength absorption changes recorded at 490 nm following pulsed 470 nm excitation for **Cu-1** (solid) and **NS-Cu-1** (dotted) in the presence of 10 mM of 4-nitrobenzene diazonium tetrafluoroborate. All experiments were carried out in argon purged solutions.

tent with the loss of the MLCT transition *via* oxidative electron transfer associated with the excited-state oxidation of Cu(I) into Cu(II) and the corresponding reduction of the aryl diazonium derivative. Such absorption changes are consistent with those observed for prototypical Ru(II) photosensitizers upon one-electron oxidation.[1t,37] Note that the reduced aryl radical does not absorb in that wavelength range. In addition, at these concentrations, the transient species perdured on the millisecond timescale, which is very promising for photocatalytic applications.

In heterogeneous conditions, a similar quenching rate constant with 4-nitrobenzene diazonium tetrafluoroborate was determined in acetonitrile, *i.e.* $3\times10^9\ M^{-1}s^{-1}$. The main challenge associated with these experiments was the dispersion efficiency of the silica nanoparticles which impacts the intensity of the photoluminescence. In addition, aggregation of silica nanoparticles could impair the photocatalyst's availability to engage in excited-state reactivity. When an effective dispersion was assured (*i.e.* no persistent solid aggregates), the heterogenized photocatalyst was capable of reacting with the aryl diazonium and thus, induced photochemical reaction at the solid surface which is, to the best of our knowledge, one of the first example in the literature using copper(I) complexes.

At this stage, it should be noted that for heterogeneous photoredox catalysis application, an oxidative quenching generating an oxidized photosensitizer might be preferable compared to a reductive pathway. Indeed, in a classical reductive pathway, the excited-state is reduced by large amount of sacrificial electron donor, whose sole purpose is to ensure a high yield of formation of the reduced species. In solution, this reduced photosensitizer then diffuses until it encounters a suitable reactive substrate, yielding the original photosensitizer and reduced substrate. This therefore depends on diffusion properties of the (reduced) photosensitizer. When heterogenized, the reduced photosensitizer does not have the possibility to diffuse, and chances of encountering the substrate are hence less probable. However, in oxidative electron transfer, the oxidized photosensitizer is formed as well as the corresponding reduced substrate, which can then diffuse out of the support and be used to drive further reactivity. If sufficiently stable, the oxidized copper can rest in that oxidized state until it finds a suitable regeneration pathway. Transient absorption experiments were also realized in heterogenous conditions and the same profile as in homogeneous conditions was observed. This is interesting as it shows that the immobilization does not seem to have an impact on the photoactivity of the complex and highlights that Cu(II) can be transiently formed. The recombination process seemed to occur faster in heterogeneous conditions than in homogeneous ones, but still lasts for several hundreds of microseconds.

Photocatalytic tests

The photoactivity of both homogeneous and heterogeneous copper complexes were investigated. To do so, an already established $[Ru(bpy)_3]^{2+}$-photocatalyzed reaction was transposed and optimized under heterogenized conditions to assess the efficiency of these copper(I) complexes for such reactions, as well as to evaluate the recyclability efficiency. The α-arylation of an enol acetate (**2a**) using 4-nitrobenzene diazonium tetrafluoroborate **1a** mediated by visible light was used as a benchmark reaction (Table 3). This reaction was reported by the Burkhard König's group to work efficiently in DMF using $[Ru(bpy)_3]^{2+}$ as photosensitizer.[38] In here, we used a LED with an emission distributed between 435 and 500 nm with a maximum centred at 470 nm. This allowed to sufficiently excite both photosensitizers (Figure S15), while higher-energy wavelength LED would lead to some undesired reactivity of the substrate so it was avoided. We were able to reproduce the reaction using $[Ru(bpy)_3]^{2+}$ as photosensitizer which yielded the desired product in 88% yield following 2 hours of irradiation. Smaller yields of 55% were obtained after 2 hours in homogeneous conditions when **Cu-2** was used as photosensitizer. This yield was increased to 78% when the irradiation time was increased to 4 hours (entry 3). In DCM, the photoactivity dropped completely, probably due to the poor solubility of 4-nitrobenzene diazonium tetrafluoroborate (entry 4). Moderate yields of 45% were obtained when **Cu-1** was used (entry 6). Control experiments highlighted that both a light source and

Table 3. Photoactivity evaluation of homogeneous and immobilized copper complexes.[a]

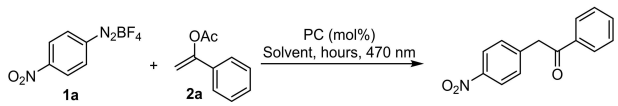

Entry	Photocatalyst (PC)	PC (mol %)	Time (h)	Solvent	Yield[b] (%)
1	$[Ru(bpy)_3](PF_6)_2$	2	2	DMF	88
2	Cu-2	5	2	DMF	55
3	Cu-2	5	4	DMF	78
4	Cu-2	5	4	DCM	8
5	Cu-1	5	2	DMF	22
6	Cu-1	5	4	DMF	45
7	Cu-1	5	16	DMF	50
8	No light	5	4	DMF	3[c]
9	No photocatalyst	–	4	DMF	1[c]
10	CS-Cu-2	5	16	DMF	14
11	NS-Cu-2	5	16	DMF	33
12	NS-Cu-2 (Run 2)	5	16	DMF	24
13	NS-Cu-1	5	16	DMF	40
14	NS-Cu-1 (Run 2)	5	16	DMF	39
15	NS-Cu-1 (Run 3)	5	16	DMF	31
16	NS-Cu-1 (Run 4)	5	16	DMF	27
17	NS-Cu-1 (Run 5)	5	16	DMF	18

[a] The reaction was performed using 0.15 mmol of **1a**, 10 equiv. of **2a** and two blue Thorlabs lamps (470 nm, 4.0 mW/cm^2, output power of 253 mW). [b] Isolated yields. [c] NMR yield using dimethylsulfone as internal standard.

the photosensitizer were needed for an efficient reaction to occur (entries 8 and 9). These results showcase the efficiency of the newly reported **Cu-2** for the α-arylation reaction while the corresponding homoleptic **Cu-1** exhibited only moderate activity in 4 hours.

Encouraged by these results, we transposed the best reaction conditions to the heterogenized copper complexes. To do so, we kept the respective ratios of photosensitizers and reagents unchanged but increased the volume of reaction from 0.4 to 10 mL to ensure optimal dispersion of the silica-supported photosensitizers. The heteroleptic copper complex immobilized on core-shell nanostructures **CS-Cu-2** gave disappointing results in the first run of reaction as only a 14% isolated yield for the product was obtained (entry 10). CS nanostructures are probably not the most suitable support as the diffusion of the reactants and the light path to the pores seem to be limiting factors in this reaction. Moreover, chemical transformations at the solid surface depend on adsorption/desorption equilibria that can also lower the overall apparent rate of the reaction compared to homogeneous conditions. Even more concerning was the orange coloration of silica nanoparticles that was clearly visualized during the nanoparticle's dispersion step, meaning that the homoleptic complex could possibly be formed just by applying ultrasound (Figure S22). Heterogenized photocatalyst on nanospheres **NS-Cu-2** gave better isolated yields of 33% (entry 11). However, the orange color of the silica nanoparticles at the end of the reaction indicated the probable formation of the homoleptic complex at the solid surface (Figure S21). Both CS and NS recovered solids were analyzed by XPS to check the presence of all elements and verify the proposed hypothesis about homoleptic complex formation (Table 4). Indeed, phosphorus was no longer detected and only the inelastic component of Si_{2p} was visualized (Figure 7). Hence, it seems that the DPEPhos ligand was completely removed during the course of the photoredox catalytic reaction.

Under oxidative conditions, Fischer *et al.* demonstrated that a heteroleptic copper complex decomposed by the dissociation of the sterically demanding phosphine ligand (elongation of the Cu–P bond and a decrease in the bite angle value). A second diimine ligand is then able to coordinate to form the homoleptic copper complex.[39] This dynamic ligand exchange was also reported by Kaeser *et al.*.[7a] Another reason for the loss in phosphorus element could be the oxidation of the DPEPhos ligand that would no longer be coordinating. The atomic ratios after the first run corresponded to the theoretical ratios expected for the homoleptic complex, validating the previously formulated hypothesis. A leaching of copper was also observed for which its surface atomic concentration was divided by half. This is consistent with the formation of the homoleptic photocatalyst as two anchored ligands are needed for one copper center. Therefore, it seems that the homoleptic complex was formed, irrespective of the morphology of the support. A regeneration attempt on NS was performed by adding fresh DPEPhos ligand at the solid surface but this approach was unfortunately not successful as no phosphorus element could be detected by XPS.

Heterogeneous tests were carried out using the immobilized homoleptic complex **NS-Cu-1**. In otherwise identical conditions, 40% isolated yields were obtained (entry 13), emphasizing that the homoleptic complex is competent for that reaction, with yields close to the one obtained in homogeneous conditions. **NS-Cu-1** were then recycled by simple filtration at the end of the reaction. The solid was washed with ~50 mL of diethyl ether and dried for several hours under high vacuum before being used in the next run of reaction. When the anchored homoleptic complex **NS-Cu-1** was used in a second run of reaction, a 39% isolated yield was obtained which is similar to the first run (entry 14). This photoactivity was maintained over 4 runs before dropping by half on the fifth run (entries 15–17). **NS-Cu-2** was used in a recycling run and a 24% isolated yield was obtained (entry 12), which is consistent with the activity of the anchored homoleptic complex, albeit with a smaller surface loading. The heterogenized homoleptic complex remained stable throughout these experiments as copper and nitrogen were still detected by XPS after these runs (Figure S29). However, a loss in these elements was observed when comparing to the initial atomic percentages of **NS-Cu-1** before use. It seems that 25% of the initial copper was still present at the surface while the leaching of the ligand was much less important as 70% of the initial nitrogen was detected. Hence, the lower amount of copper present at

Table 4. XPS atomic ratios of **NS-Cu-1** and **NS-Cu-2** and of the recovered heterogenized heteroleptic and homoleptic complexes after the first run of reaction.

Atomic ratios	NS-Cu-1	NS-Cu-1 Run 1	NS-Cu-2	NS-Cu-2 Run 1
N/Si	0.09	0.07	0.11	0.08
N/C	0.13	0.19	0.08	0.15
Cu/C	0.018	0.013	0.02	0.03
Cu/N	0.14	0.07	0.32	0.18
Cu/P	–	–	1.40[a]	–
Cu/F	0.23	0.04	0.25	0.04
P/F[b]	–	–	0.04	–

[a] Only the phosphine component was used. [b] Only the phosphorus component arising from the counteranion was used.

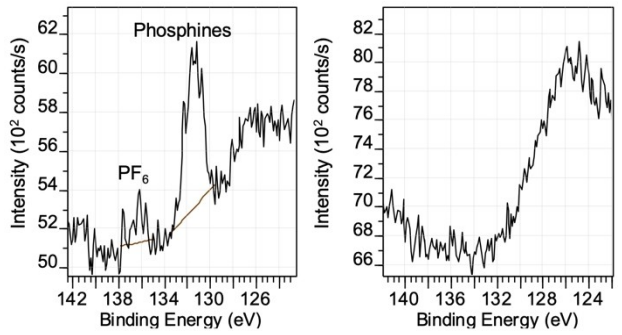

Figure 7. P_{2p} XPS spectra of **NS-Cu-2** (left) and **NS-Cu-2** after photocatalyzed α-arylation of enol acetate **2a** (right).

the NS surface explains the smaller isolated yields in the fifth run.

All samples were also characterized by DR-UV-vis to further prove our hypothesis of the *in situ* formation of homoleptic complex. After one run of reaction using the heterogenized heteroleptic complex, an absorption profile similar to that of the homoleptic complex was clearly observed (Figure S30).

Conclusions

In conclusion, a robust strategy for the functionalization of silica nanospheres with homoleptic and heteroleptic copper(I) complexes was reported. In one step, heterogenized copper complexes were obtained that maintained photophysical properties compatible with excited-state reactivity. Stern-Volmer analysis revealed that aryl diazonium derivatives were suitable reagents for excited-state oxidative electron transfer that were used to trigger a reported α-arylation of enol acetate reaction. The homogeneous and heterogeneous homoleptic complexes were able to perform that reaction with moderate yields. Importantly, the supported photocatalyst could be efficiently recovered and the photocatalytic activity was maintained with slightly altered yields over 4 runs. Unfortunately, the heteroleptic complex, whether in homogeneous solution or heterogenized on silica nanospheres did not exhibit sufficient photostability and underwent the well-known ligand exchange to form the corresponding homoleptic derivatives. Nanosecond transient absorption spectroscopy revealed that both **Cu-1** and **NS-Cu-1** were competent for excited-state electron transfer to 4-nitrobenzene diazonium tetrafluoroborate that generated the corresponding Cu(II) analogue that persisted on the millisecond timescale. The nearly retained photophysical properties of the anchored homoleptic complex are promising for other applications in photoredox catalysis and solar fuel productions. In addition, photocatalytic yields were almost unchanged in homogeneous and heterogenous conditions. That aspect, coupled to the developed methodology that yields robust functionalized surfaces, highlight that the anchoring methodology is optimal but that better copper(I) photosensitizer could be useful to burst the door open to efficient and recyclable photocatalysts.[3i]

Experimental Section

Chemicals and materials: All reactions were carried out using flame-dried glassware and magnetic stirring under an argon atmosphere unless otherwise stated. Commercial reagents were used as received while dichloromethane and toluene were distilled on MBraun MBSPS5 device before use. Ethanol (99% V/V euro denaturated with 1% of isopropanol), tetraethylorthosilicate (TEOS, ≥99%, Sigma-Aldrich), ammonium hydroxide (NH_4OH, 25% solution in water, Acros Organics), hexadecyltrimethylammonium bromide (CTAB, ≥99%, Sigma Aldrich), anhydrous chloroform (≥99% with 0.5–1.0% ethanol as stabilizer, Sigma-Aldrich), anhydrous dimethylformamide (99.8%, Sigma-Aldrich), 2,9-dimethyl-1,10-phenanthroline (≥98%, Sigma-Aldrich), palladium on activated carbon (5% Pd, Acros Organics), hydrazine hydrate ($N_2H_4.H_2O$, 99.9%, Acros Organics), triethoxy(3-isocyanatopropyl)silane (95%, ABCR), DPEPhos (99%, Acros Organics), tetrakis(acetonitrile)copper(I) hexafluorophosphate (>97%, TCI), acetophenone (98%, Acros Organics), isopropenyl acetate (99%, Sigma-Aldrich), *p*-toluenesulfonic acid (*p*-TsOH, >98%, Sigma-Aldrich), 4-nitrobenzenediazonium tetrafluoroborate (>98%, TCI) were commercially available and used as received. 2,9-dimethyl-5-nitro-1,10-phenanthroline (DMP-NO_2),[40] 2,9-dimethyl-5-amino-1,10-phenanthroline (DMP-NH_2),[40] [Cu-(DPEPhos)$_2$]PF_6[41] and 1-phenylvinyl acetate[38] were synthesized according to published literature.

Characterization methods

Nuclear magnetic resonance (NMR): NMR spectra were recorded on BRUKER spectrometers (300 MHz for ^{1}H, 75 MHz for ^{13}C, 121 MHz for ^{31}P). Chemical shifts are reported in δ ppm relative to either the residual solvent peak of $CDCl_3$ (δ = 7.26 ppm) or the signal of PF_6^- (δ = −144.30 ppm). The following abbreviations have been used: δ (chemical shift), *J* (coupling constant expressed in hertz), br (broad), s (singlet), d (doublet), t (triplet), q (quadruplet) and m (multiplet).

X-Ray photoelectron spectroscopy (XPS): XPS analyses were carried out at room temperature with a SSIX-probe (SSX 100/206) photoelectron spectrometer from Surface Science Instruments (USA) equipped with a monochromatized microfocus Al X-ray source. Samples were stuck onto small sample holders with double-face adhesive tape and then placed on an insulating home-made ceramic carousel (Macor®, Switzerland). Charge effects were avoided by placing a nickel grid above the samples and using a flood gun set at 8 eV. The binding energies were calculated with respect to the Si_{2p} peak fixed at 103.5 eV. Data treatment was performed with the CasaXPS program (Casa Software Ltd., UK). The peaks were decomposed into a sum of Gaussian/Lorentzian (85/15) after subtraction of a Shirley type baseline.

UV-vis: UV-vis absorption spectra were recorded on a Shimadzu UV-1700 instrument using 1 cm large cuvettes in quartz.

Photostability: A cuvette or an NMR tube containing the investigated copper complex dissolved in DMF or deuterated DMF was irradiated with two Thorlabs 470 nm LEDs (Figure S31 for setup). After specific time intervals, the cuvette was transported to an Agilent Cary 60 spectrophotometer and an absorption spectrum was recorded. To do that, the apparatus recorded the transmittance from 800 to 300 nm with a scan rate of 600 nm/min with a data interval of 1.00 nm and an average time of 0.1 s. Control experiments (Figure S32) showed that the Agilent Cary 60 spectrophotometer source had no impact on the photodegradation. Alternatively, the NMR tube was carried to the NMR facility and a ^{1}H NMR spectrum was recorded.

Photoluminescence: Time-resolved photoluminescence spectra were recorded on a LP980-K spectrometer from Edinburgh Instruments (see nanosecond transient absorption for full description). The optically diluted samples were excited with pulsed light and the excited-state lifetime was measured on a PMT LP detector (Hamamatsu R928) which covers the spectral range from 185 to 870 nm. An average of 30 scans per measurement was used.

Cyclic voltammetry (CV) and differential pulse voltammetry (DPV): Experiments were performed with an Autolab PGSTAT 100 potentiostat using a standard three-electrode-cell, *i.e.* a glassy carbon disk working electrode (approximated area = 0.03 cm^2), a platinum wire counter electrode and an aqueous Ag/AgCl reference electrode (salt bridge: 3 M KCl/saturated AgCl). Experiments were performed in 0.1 M tetrabutylammonium hexafluorophosphate acetonitrile electrolyte, and the samples were purged with argon before each measurement.

Nanosecond transient absorption: Nanosecond transient absorption measurements were recorded on a previously described apparatus.[1t] Briefly, the latter consisted in a LP980-K spectrometer from Edinburgh Instruments equipped with an iCCD detector from Andor (DH320T). The excitation source was a tunable Nd:YAG Laser NT342 Series from EKSPLA. The third harmonic (355 nm) at 150 mJ was directed into an optical parametric oscillator (OPO) to enable wavelength tuning starting from 410 nm. The laser power was then attenuated to reach appreciable signal/noise and the integrity of the samples was verified by UV–Vis measurements. The LP980-K is equipped with a symmetrical Czerny-Turner monochromator. For single wavelength absorption changes, a 1800 g mm^{-1} grating, blazed at 500 nm is used, which affords wavelength coverage from 200 to 900 nm. For spectral mode (iCCD), a 150 g mm^{-1} grating, blazed at 500 nm is used, offering a wavelength coverage of 540 nm over the full wavelength range extending from 250 to 900 nm. Single wavelength absorption changes were monitored using a PMT LP detector (Hamamatsu R928) which covers the spectral range from 185 to 870 nm. The probe was a 150 W ozone-free xenon short arc lamp (OSRAM XBO 150 W/CR OFR) that was pulsed at the same frequency of the laser. The excitation wavelength depended on the photosensitizers but in all cases the concentration at the excitation wavelength was adjusted to reach absorbance values between 0.3 and 0.5. All measurements were performed in argon-purged solvents at room temperature. An average of 30 to 90 scans per measurement was used.

Stern-Volmer: Stern-Volmer experiments were performed in a quartz cuvette equipped with a 24/32 joint. Cuvettes were sealed with Teflon tape, a septum and parafilm. All samples were purged with dried argon, that was passed through a bubbler containing the solvent of interest, for at least 15 minutes. *p*-nitrobenzenediazonium tetrafluoroborate stock solutions with a concentration of ~11 mM were prepared in 10 mL of dry acetonitrile. In dichloromethane, the concentration was ~0.6 mM as the *p*-nitrobenzenediazonium tetrafluoroborate is only slightly soluble. A photosensitizer solution with an absorbance of ~0.2 at the excitation wavelength was prepared in dry acetonitrile or dichloromethane. The desired *p*-nitrobenzenediazonium tetrafluoroborate quencher was then gradually added to the photosensitizer cuvette. The excited-state quenching was monitored by time-resolved spectroscopy using the LP980-K spectrometer from Edinburgh Instruments (see above). The decrease of excited-state lifetime is directly related to the concentration of quencher and the respective Stern-Volmer plots were extrapolated using the following equation. The quenching rate constant (k_q) was then determined by dividing the slope by the initial lifetime without any quencher.

$$\frac{\sum(PLI_0)}{\sum(PLI)} = \frac{\tau_0}{\tau} = 1 + K_{SV}[Q] \; = 1 + k_q\tau_0[Q] \qquad (1)$$

Thermogravimetric analysis (TGA): Thermograms were recorded on a TGA/SDTA 851e simultaneous DSC-TGA instrument from METTLER TOLEDO. These analyses were carried out with a heating ramp of 10 °C min^{-1} and under air flow (100 mL min^{-1}) with the samples (3–20 mg) placed into alumina containers.

Transmission electron microscopy (TEM): TEM images were obtained with a LEO 922 OMEGA energy filter transmission electron microscope. The powder samples were suspended in ethanol under ultrasonic treatment, then a few drops of the supernatant were deposited on a holey carbon film supported on a copper grid (Protochips, 1.2 micron hole diameter, 1.3 micron hole spacing, 200 mesh copper grid), which was dried for a few hours under vacuum at room temperature before analysis.

Fourier-transform infrared total attenuated reflectance spectroscopy (FTIR-ATR): FTIR-ATR spectra were recorded on Perkin Elmer Spectrum Two-UATR by depositing the powder onto the diamond equipped with a mechanical press. The bands are reported in cm^{-1} and the following abbreviations have been used: br (broad), s (strong), m (medium), w (weak).

Diffuse reflectance-UV-vis (DR-UV-vis): DR-UV-vis spectra were recorded on a Shimadzu 2600plus device from 800 to 200 nm using a harrick praying mantis modulus. Spectralon was used to record the baseline prior to powder samples measurements.

Time of flight secondary ion mass spectrometry (ToF-SIMS): Chemical characterisation of samples were carried out by using a TOF.SIMS 5 instrument (IONTOF GmbH, Münster, Germany). A pulsed Bi^{5+} metal ion source was used to produce a primary beam using an acceleration voltage of 30 kV. An AC target current of 0.05 pA with a bunched pulse width lower than 1 ns was used. Both positive and negative secondary ion species were analysed. For spectra, a raster of 128×128 data points over an area of 300×300 μm^2 was recorded. The total primary ion beam dose for each analysed area was always kept below 4×10^{10} ions.cm^{-2}, ensuring static conditions. Lateral resolution of ~3 μm and mass resolution m/Δm > 5000 at 41 m/z were maintained for positive and negative spectra acquisition. Charge compensation was done by an interlaced electron flood gun (Ek = 20 eV). All data analyses were carried out using the software supplied by the instrument manufacturer, SurfaceLab (version 6.8). Sample powders were simply pressed onto the adhesive part of Post-it® papers before introduction in the instrument.

Inductively coupled plasma optical emission spectroscopy (ICP-OES): These analyses were performed by MEDAC LTD company using Varian Vista MPX ICP-OES system. The sample was digested using a combination of HNO_3 and HF acids and the mixture was made up to 100 mL of de-ionised water. A matrix blank was prepared at the sample time.

High resolution mass spectrometry: HRMS were recorded on a Q-Extractive orbitrap from ThermoFisher. Samples were ionized by Electrospray Ionization (ESI) (capillary temperature: 250 °C, vaporizer temperature: 250 °C, sheath gas flow rate: 20).

Nitrogen physisorption: The specific surface areas were measured by nitrogen adsorption-desorption isotherms. The measurements were achieved using a Micromeritics ASAP 2020 analyzer at −196 °C. Before analysis, the samples (~200 mg) were degassed for 2 h at 200 °C with a heating ramp of 10 °C min^{-1} under 0.133 Pa pressure. The analysis of the isotherms provided specific surface areas calculated with the Brunauer-Emmett-Teller (BET) equation.

Synthesis of 2,9-dimethylphenanthroline-siloxane ligand (DMP-Si). 2,9-dimethyl-5-amino-1,10-phenanthroline (100 mg, 0.45 mmol, 1 eq.) and molecular sieves were added in a 25 mL two-neck round-bottom flask. The flask was placed under static vacuum for 10 minutes and filled with argon. 5 mL of dry chloroform were added followed by the dropwise addition of triethoxy(3-isocyanatopropyl)silane (0.11 mL, 0.45 mmol, 1 eq.). The reaction mixture was heated at 80 °C for 16 h. After reaction, the solvent was evaporated under reduced pressure and the crude residue was purified by silica flash chromatography (DCM/MeOH, 100:0 to 95:5). The DMP-Si ligand was obtained as a brown oil (138 mg, 65% yield). ^{1}H NMR (300 MHz, $CDCl_3$): δ = 9.07 (br, 1H), 8.42 (s, 1H), 8.24 (d, *J* = 8.6 Hz, 1H), 8.09 (d, *J* = 8.3 Hz, 1H), 7.42 (d, *J* = 8.3 Hz, 1H), 6.77 (m, 2H), 3.62 (q, *J* = 7.0 Hz, 6H), 3.30 (m, 2H), 2.78 (s, 3H), 2.51 (s, 3H), 1.54 (m, 2H), 1.06 (t, *J* = 7.0 Hz, 9H), 0.49 (t, *J* = 8.4 Hz, 2H); ^{13}C NMR (75 MHz, $CDCl_3$): δ = 158.6, 157.7, 156.9, 145.4, 142.2, 136.4, 132.9, 131.0, 127.7, 124.3, 122.8, 122.5, 114.5, 58.4, 42.7, 24.8, 24.5, 23.7, 18.3, 7.7; IR (cm^{-1}): $\tilde{\nu}$ = 3322 (m), 2973 (m), 2926 (m), 1656 (m),

1102 (s), 1078 (s), 954 (m); HRMS (ESI) *m/z* calcd for $C_{24}H_{34}O_4N_4{}^{28}Si+H^+$: 471.2422 $[M+H]^+$; found: 471.2424.

Synthesis of [Cu(DMP-Si)(DPEPhos)]PF_6 (Cu-2). In two flame-dried 25 mL round-bottom flasks, $[Cu(DPEPhos)_2]PF_6$ (140 mg, 0.3 mmol, 1 eq.) and DMP-Si ligand (386 mg, 0.3 mmol, 1 eq.) were added separately. The flasks were placed under static vacuum for 10 minutes and filled with argon. The copper complex was dissolved in 20 mL of dry dichloromethane and a minimum amount of dichloromethane was added to solubilize the DMP-Si ligand. The solution of DMP-Si was cannula-transferred to the copper solution leading to an immediate orange/yellow color. The reaction medium was left under stirring for one hour under the dark. After reaction, the mixture was added dropwise to 100 mL of *n*-hexane previously cooled to 0 °C. The yellow precipitate was recovered by filtration. If free DPEPhos was still observed by NMR spectroscopy, the copper complex was purified by silica flash chromatography (3% methanol in dichloromethane). The title compound **Cu-2** was obtained as a yellow solid (95 mg, 61% yield). ^{1}H NMR (300 MHz, $CDCl_3$): δ = 8.75 (d, J = 8.7 Hz, 1H), 8.35 (s, 1H), 8.11 (d, J = 8.3 Hz, 1H), 7.69 (s, 1H), 7.54 (d, J = 8.6 Hz, 1H), 7.35 (d, J = 8.2 Hz, 1H), 7.33–7.28 (m, 2H), 7.25–7.13 (m, 8H), 7.08–6.87 (m, 18H), 5.92 (t, J = 5.8 Hz, 1H), 3.84 (q, J = 7.0 Hz, 6H), 3.33 (q, J = 6.7 Hz, 2H), 2.37 (s, 3H), 2.34 (s, 3H), 1.75 (m, 2H), 1.23 (t, J = 7.0 Hz, 9H), 0.80–0.68 (m, 2H); ^{31}P NMR (121 MHz, $CDCl_3$): δ = −13.33, −126.66, −132.54, −138.42, −144.30, −150.18, −156.06, −161.94; ^{13}C NMR (75 MHz, $CDCl_3$): δ = 158.5, 158.4, 156.2, 156.0, 143.4, 140.2, 137.2, 133.9, 133.8, 133.2, 133.1, 132.8, 132.2, 131.7, 130.1, 128.7, 128.7, 128.4, 125.7, 125.3, 125.2, 125.0, 123.3, 120.2, 114.2, 58.5, 43.2, 27.1, 27.0, 23.4, 18.5, 7.6; IR (cm^{-1}): $\tilde{\nu}$ = 3427, (br), 2926 (m), 1657 (s), 1462 (m), 1435 (s), 1097 (s), 1066 (s), 956 (s), 833 (s), 740 (s), 697 (s); HRMS (ESI): *m/z* calcd for $C_{60}H_{62}O_5N_4{}^{63}CuP_2{}^{28}Si$: 1071.3255 $[M-PF_6]^+$; found: 1071.3272.

Synthesis of [Cu(DMP-Si)$_2$]PF_6 (Cu-1). $[Cu(MeCN)_4]PF_6$ (37 mg, 0.1 mmol, 1 eq.) was added in a 50 mL flame-dried round-bottom flask. The flask was placed under static vacuum for 10 minutes and filled with argon. 13 mL of dry dichloromethane was added and a solution of DMP-Si (94 mg, 0.2 mmol, 2 eq.) in dichloromethane was added dropwise. A red color was observed that went darker along the time of reaction. The reaction mixture was left under stirring for 1 hour under the dark. After reaction, the solvent was evaporated under reduced pressure. The crude residue was dissolved in a minimum amount of dichloromethane and added dropwise in 100 mL of *n*-hexane previously cooled to 0 °C. An orange/red powder corresponding to complex **Cu-1** was recovered by filtration (65 mg, 57% yield). ^{1}H NMR (300 MHz, $CDCl_3$): δ = 8.72 (br, 2H), 8.37 (br, 2H), 8.23 (br, 2H), 7.78 (br, 2H), 7.57 (m, 4H), 5.97 (br, 2H), 3.83 (q, J = 7.0 Hz, 12H), 3.33 (br, 4H), 2.34 (s, 6H), 2.25 (s, 6H), 1.74 (m, 4H), 1.21 (t, J = 7.0 Hz, 18H), 0.72 (m, 4H); ^{13}C NMR (75 MHz, $CDCl_3$): δ = 156.9, 156.0, 155.4, 143.4, 140.1, 136.4, 133.4, 132.3, 128.1, 125.4, 124.9, 119.6, 115.2, 58.5, 43.1, 25.7, 25.4, 23.4, 18.3, 7.6; IR (c^{-1}): $\tilde{\nu}$ = 3373 (m), 2927 (m), 1655 (s), 1102 (s), 1073 (s), 956 (s), 835 (s), 775 (s); HRMS (ESI): *m/z* calcd for $C_{48}H_{68}O_8N_8{}^{63}Cu^{28}Si_2$: 1003.3989 $[M-PF_6]^+$; found: 1003.3986.

Silica nanospheres (NS) synthesis. Reaction conditions were adapted from the work of Stöber *et al.* to yield bigger quantities of silica nanospheres.[29] 150 mL of ethanol (99.9% denaturated) were introduced in a 500 mL Erlenmeyer. Under vigorous stirring, 6 mL of NH_4OH were added. The reaction mixture was stirred for 5 min at room temperature. Then, 10 mL of tetraethylorthosilicate (TEOS) were added dropwise with a syringe pump at a rate of 59 mL hour^{-1}. The solution was left under stirring for 6 hours at room temperature. The silica nanoparticles were recovered by centrifugation (9.500 rpm for 40 min) and washed three times with 40 mL of ethanol. The nanoparticles were dried in the oven at 100 °C overnight and subsequently grinded to obtain a fine white/beige powder. This material was characterized by TEM, XPS and BET.

Silica Core-Shell (CS) nanoparticles synthesis. Reaction conditions were adapted from the work of Yoon *et al.* to yield smaller nanoparticles.[30] 150 mL of ethanol (99.9% denaturated) were introduced in a 500 mL Erlenmeyer. Under vigorous stirring, 6 mL of NH_4OH were added. The reaction mixture was stirred for 5 min at room temperature. Then, 10 mL of tetraethylorthosilicate (TEOS) were added dropwise with a syringe pump at a rate of 59 mL hour^{-1}. The solution was left under stirring for 6 hours at room temperature. 380 mL of Milli-Q water and 30 mL of a hexadecyltrimethylammonium bromide (CTAB) solution (1.2 g of CTAB dissolved in 20 mL H_2O/10 mL ethanol) were added and the solution was left under stirring for 30 min. 2.15 mL of TEOS were added and the mixture was stirred overnight. The silica nanoparticles were recovered by centrifugation (6000 rpm for 50 min) and washed three times with 40 mL of ethanol. The nanoparticles were dried in the oven at 100 °C and finally calcinated by heating at 500 °C for 5 hours at a rate of 10 °C min^{-1} (3 g of silica nanoparticles were recovered). This material was characterized by TEM, XPS and BET.

Anchoring of [Cu(DMP-Si)(DPEPhos)]PF_6 (Cu-2) according to a two-step procedure. In a flame-dried 25 mL two-neck round-bottom flask were inserted silica core-shell nanoparticles (100 mg). The flask was placed under static vacuum for 10 minutes and filled with argon. 5 mL of dry toluene were added and the resulting suspension was sonicated for 15 min at power 3 on a VWR ultrasonic bath. DMP-Si ligand (94 mg, 0.2 mmol, 0.12 eq.) was dissolved in 5 mL of toluene before being added dropwise at a rate of 8 mL hour^{-1}. The reaction mixture was refluxed at 120 °C for 24 h. Filtration on a PVDF Millipore Membrane (0.1 μm) allowed the recovery of a yellowish solid which was washed several times with absolute ethanol. The functionalized core-shell nanoparticles were then added in a 25 mL flame-dried round-bottom flask. The flask was placed under static vacuum for 10 minutes and filled with argon. 8.5 mL of dry dichloromethane was added to the silica nanoparticles and the resulting suspension was sonicated for 15 minutes at power 2 on a VWR ultrasonic bath. $[Cu(DPEPhos)_2]PF_6$ (93 mg, 0.07 mmol) was placed in a round-bottom flask and the latter was placed under static vacuum for 10 minutes and filled with argon. 1.5 mL of dry dichloromethane were added and this solution was added dropwise to the silica nanoparticles suspension that was stirred at ambient temperature for an additional 16 h. The solid was recovered by filtration on a PVDF Millipore Membrane (0.1 μm) and washed three times with 10 mL of dichloromethane. The resulting yellowish powder was dried under vacuum for several hours.

General one-step procedure for the anchoring of copper complexes. In a 50 mL flame-dried two-neck round-bottom flask, nanospheres or core-shell nanoparticles (140 mg) were introduced. The flask was placed under static vacuum for 10 minutes before being filled with argon. 30 mL of dry toluene were added and the resulting suspension was sonicated for 15 minutes at power 2 on a VWR ultrasonic bath. The homoleptic or heteroleptic copper complexes (90 mg and 100 mg, respectively, 0.08 mmol) were dissolved in a minimum amount of dry toluene and added dropwise to the silica suspension. The suspension was refluxed for 24 h. After reaction, the mixture was cooled to room temperature and filtered on a PVDF Millipore Membrane (0.1 μm). The powder was recovered and washed three times with 10 mL of dichloromethane. The solid was dried under vacuum for several hours.

Use of homogeneous photocatalysts for the α-arylation of 1-phenylvinyl acetate 2 a. In a 3 mL oven-dried vial were dissolved 4-nitrobenzene diazonium tetrafluoroborate 1a (35.5 mg, 0.15 mmol,

1 eq.), 1-phenylvinyl acetate 2a (243 mg, 1.5 mmol, 10 eq.) and the photocatalyst (2–5 mol%) in 0.4 mL of dry dimethylformamide. Argon was bubbled for 15 min and the solution was irradiated for 2 or 4 hours (depending on the photocatalyst) with two LIU470A 470 nm blue LEDs purchased from Thorlabs (intensity = 4.0 mW/cm^2; total output power = 253 mW; supply voltage = 24 V). After reaction, 5 mL of distilled water were added and the aqueous phase was washed three times with 10 mL of diethylether. The organic phases were combined, dried over $MgSO_4$, filtered and the solvent was evaporated under reduced pressure. The crude residue was purified over silica flash chromatography using NextGen Combi-Flash device along with 12 g silica column (*n*-hexane/ethyl acetate). The following gradient in ethyl acetate was used: 0 to 2.5% (2 min), 2.5% (1 min), 2.5 to 5% (1 min), 5% (2 min), 5 to 7.5% (1 min), 7.5% (1 min), 7.5 to 10% (1 min), 10% (2 min). The product was recovered as a white powder. ^{1}H NMR (300 MHz, $CDCl_3$): δ = 8.25–8.14 (m, 2H), 8.06–7.96 (m, 2H), 7.66–7.56 (m, 1H), 7.55–7.47 (m, 2H), 7.45–7.40 (m, 2H), 4.42 (s, 2H); ^{13}C NMR (75 MHz, $CDCl_3$): δ = 196.1, 147.2, 142.2, 136.3, 133.9, 130.8, 129.0, 128.6, 123.9, 45.1; IR (cm^{-1}): $\tilde{\nu}$ = 2922 (w), 1683 (s), 1599 (m), 1514 (s), 1108 (m), 993 (m), 761 (s), 733 (s), 690 (s).

Use of heterogeneous photocatalysts for the α-arylation of 1-phenylvinyl acetate 2 a. In a 50 mL flame-dried round-bottom flask, the heterogenized copper complex (50 mg for homoleptic and 65 mg for heteroleptic) was introduced and placed under static vacuum for 10 minutes before being filled with argon. 8–10 mL of degassed (freeze-pump-thaw) dry dimethylformamide were added and the resulting suspension was sonicated for 15 minutes at power 2 on a VWR ultrasonic bath. 4-nitrobenzene diazonium tetrafluoroborate 1a (35.5 mg, 0.15 mmol, 1 eq.) and 1-phenylvinyl acetate 2a (243 mg, 1.5 mmol, 10 eq.) were added and the suspension was left under stirring for 16 h at room temperature under blue irradiation. After reaction, the heterogenized copper complex was recovered by filtration on a PTFE Millipore Membrane (0.1 μm) and the solid was washed three times with 10 mL of diethylether. To the filtrate was added 20 mL of distilled water and the aqueous phase was washed three times with 20 mL of diethylether. The organic phases were combined, washed with saturated NaCl (20 mL) and LiCl 10% (20 mL), dried over $MgSO_4$, filtered and the solvent was evaporated under reduced pressure. The white powder was finally dried under vacuum.

Acknowledgements

NB, SH and L.T.-G. thank the Belgian National Funds for Scientific Research (F.R.S.-FNRS) for their Fund for Research Training in Industry and Agriculture (FRIA) PhD grant, Research Director and chercheur qualifié positions, respectively. NB thanks the Région Wallonne for its participation in the FRIA scheme. RB, CL, SH, OR and IJ thank INNOVIRIS for the funding of a BRIDGE project entitled "PhotoCop: Sustainable Photocatalysis with Copper Complexes" (ref: RBC (Région Bruxelles-Capitale)/2019-BRIDGE-5d). The authors thank Pierre Eloy and François Devred for their precious assistance in XPS analyses and the DR-UV-vis analyses, respectively. They also thank Claude Poleunis for the ToF-SIMS analyses. Finally, they thank Dr. S. Ouk for his generous financial support through the Fondation Louvain allowing the purchase of a solvents purification system. They are also grateful to Prof. Benjamin Elias and the corresponding grant (no. U.N021.21) for the access to nanosecond transient absorption spectroscopy.

Conflict of Interests

The authors declare no conflict of interest

Data Availability Statement

The data that support the findings of this study are available in the supplementary material of this article.

Keywords: copper · electron transfer · photoredox catalysis · recyclability · silica nanoparticles

[1] a) D. B. Bagal, G. Kachkovskyi, M. Knorn, T. Rawner, B. M. Bhanage, O. Reiser, *Angew. Chem. Int. Ed.* **2015**, *54*, 6999–7002; b) T. Rawner, E. Lutsker, C. A. Kaiser, O. Reiser, *ACS Catal.* **2018**, *8*, 3950–3956; c) F. Glaser, O. S. Wenger, *JACS Au* **2022**, *2*, 1488–1503; d) W. Leis, M. A. Argüello Cordero, S. Lochbrunner, H. Schubert, A. Berkefeld, *J. Am. Chem. Soc.* **2022**, *144*, 1169–1173; e) A. Aydogan, R. E. Bangle, S. De Kreijger, J. C. Dickenson, M. L. Singleton, E. Cauët, A. Cadranel, G. J. Meyer, B. Elias, R. N. Sampaio, L. Troian-Gautier, *Catal. Sci. Technol.* **2021**, *11*, 8037–8051; f) A. Aydogan, R. E. Bangle, A. Cadranel, M. D. Turlington, D. T. Conroy, E. Cauët, M. L. Singleton, G. J. Meyer, R. N. Sampaio, B. Elias, L. Troian-Gautier, *J. Am. Chem. Soc.* **2021**, *143*, 15661–15673; g) A. Ilic, J. Schwarz, C. Johnson, L. H. M. de Groot, S. Kaufhold, R. Lomoth, K. Wärnmark, *Chem. Sci.* **2022**, *13*, 9165–9175; h) O. S. Wenger, *J. Am. Chem. Soc.* **2018**, *140*, 13522–13533; i) J. Beaudelot, S. Oger, S. Peruško, T.-A. Phan, T. Teunens, C. Moucheron, G. Evano, *Chem. Rev.* **2022**, *122*, 16365–16609; j) C. B. Larsen, O. S. Wenger, *Chem. Eur. J.* **2018**, *24*, 2039–2058; k) J. M. R. Narayanam, C. R. J. Stephenson, *Chem. Soc. Rev.* **2011**, *40*, 102–113; l) J. A. Kübler, B. Pfund, O. S. Wenger, *JACS Au* **2022**, *2*, 2367–2380; m) S. Das, C. Zhu, D. Demirbas, E. Bill, C. K. De, B. List, *Science* **2023**, *379*, 494–499; n) N. A. Romero, D. A. Nicewicz, *Chem. Rev.* **2016**, *116*, 10075–10166; o) C. Jacob, H. Baguia, A. Dubart, S. Oger, P. Thilmany, J. Beaudelot, C. Deldaele, S. Peruško, Y. Landrain, B. Michelet, S. Neale, E. Romero, C. Moucheron, V. Van Speybroeck, C. Theunissen, G. Evano, *Nat. Commun.* **2022**, *13*, 560; p) B. Michelet, C. Deldaele, S. Kajouj, C. Moucheron, G. Evano, *Org. Lett.* **2017**, *19*, 3576–3579; q) M. Rentschler, P. J. Boden, M. A. Argüello Cordero, S. T. Steiger, M.-A. Schmid, Y. Yang, G. Niedner-Schatteburg, M. Karnahl, S. Lochbrunner, S. Tschierlei, *Inorg. Chem.* **2022**, *61*, 12249–12261; r) Y. Yang, F. Doettinger, C. Kleeberg, W. Frey, M. Karnahl, S. Tschierlei, *Front. Chem.* **2022**, *10*, 936863; s) N. Hoffmann, *ChemSusChem* **2012**, *5*, 352–371; t) A. Ripak, S. De Kreijger, R. N. Sampaio, C. A. Vincent, É. Cauët, I. Jabin, U. K. Tambar, B. Elias, L. Troian-Gautier, *Chem Catal.* **2023**, *3*, 100490.

[2] J.-M. Kern, J.-P. Sauvage, *J. Chem. Soc. Chem. Commun.* **1987**, 546–548.

[3] a) M. Pirtsch, S. Paria, T. Matsuno, H. Isobe, O. Reiser, *Chem. Eur. J.* **2012**, *18*, 7336–7340; b) X.-J. Tang, W. R. Dolbier Jr, *Angew. Chem. Int. Ed.* **2015**, *54*, 4246–4249; c) Z. Zhang, X. Tang, C. S. Thomoson, W. R. Dolbier Jr, *Org. Lett.* **2015**, *17*, 3528–3531; d) G. Fumagalli, P. T. G. Rabet, S. Boyd, M. F. Greaney, *Angew. Chem. Int. Ed.* **2015**, *54*, 11481–11484; e) M. S. Lazorski, F. N. Castellano, *Polyhedron* **2014**, *82*, 57–70; f) M. C. Rosko, K. A. Wells, C. E. Hauke, F. N. Castellano, *Inorg. Chem.* **2021**, *60*, 8394–8403; g) R. Fayad, A. T. Bui, S. G. Shepard, F. N. Castellano, *ACS Appl. Energ. Mater.* **2020**, *3*, 12557–12564; h) R. S. Khnayzer, C. E. McCusker, B. S. Olaiya, F. N. Castellano, *J. Am. Chem. Soc.* **2013**, *135*, 14068–14070; i) M. C. Rosko, E. M. Espinoza, S. Arteta, S. Kromer, J. P. Wheeler, F. N. Castellano, *Inorg. Chem.* **2023**, *62*, 3248–3259.

[4] a) S. Paria, O. Reiser, *ChemCatChem* **2014**, *6*, 2477–2483; b) Y. Zhang, M. Schulz, M. Wächtler, M. Karnahl, B. Dietzek, *Coord. Chem. Rev.* **2018**, *356*, 127–146.

[5] D. G. Cuttell, S.-M. Kuang, P. E. Fanwick, D. R. McMillin, R. A. Walton, *J. Am. Chem. Soc.* **2002**, *124*, 6–7.

[6] a) M. Zhong, Y. Gagné, T. O. Hope, X. Pannecoucke, M. Frenette, P. Jubault, T. Poisson, *Angew. Chem.* **2021**, *133*, 14619–14624; b) C. Cruche, W. Neiderer, S. K. Collins, *ACS Catal.* **2021**, *11*, 8829–8836; c) A. C. Hernandez-Perez, S. K. Collins, *Angew. Chem. Int. Ed.* **2013**, *52*, 12696–12700; d) T. P. Nicholls, J. C. Robertson, M. G. Gardiner, A. C. Bissember, *Chem. Commun.* **2018**, *54*, 4589–4592; e) T. P. Nicholls, A. C. Bissember, *Tetrahedron Lett.* **2019**, *60*, 150883; f) C. Deldaele, B. Michelet, H. Baguia,

S. Kajouj, E. Romero, C. Moucheron, G. Evano, *Chimia* **2018**, *72*, 621–629; g) A. Hossain, A. Bhattacharyya, O. Reiser, *Science* **2019**, *364*, eaav9713.
[7] a) A. Kaeser, M. Mohankumar, J. Mohanraj, F. Monti, M. Holler, J.-J. Cid, O. Moudam, I. Nierengarten, L. Karmazin-Brelot, C. Duhayon, B. Delavaux-Nicot, N. Armaroli, J.-F. Nierengarten, *Inorg. Chem.* **2013**, *52*, 12140–12151; b) D. V. Scaltrito, D. W. Thompson, J. A. O'Callaghan, G. J. Meyer, *Coord. Chem. Rev.* **2000**, *208*, 243–266; c) S.-M. Kuang, D. G. Cuttell, D. R. McMillin, P. E. Fanwick, R. A. Walton, *Inorg. Chem.* **2002**, *41*, 3313–3322.
[8] a) P. Xiao, F. Dumur, J. Zhang, J. P. Fouassier, D. Gigmes, J. Lalevee, *Macromolecules* **2014**, *47*, 3837–3844; b) Y. Zhang, M. Heberle, M. Wächtler, M. Karnahl, B. Dietzek, *RSC Adv.* **2016**, *6*, 105801–105805; c) M. Nishikawa, D. Kakizoe, Y. Saito, T. Ohishi, T. Tsubomura, *B. Chem. Soc. Jpn.* **2017**, *90*, 286–288.
[9] M. S. Lazorski, R. H. Gest, C. M. Elliott, *J. Am. Chem. Soc.* **2012**, *134*, 17466–17469.
[10] a) C. Chen, A. Chen, X. Huang, R. Ju, X. Li, J. Wang, A. Hao, M. Zhao, *J. Cleaner Prod.* **2021**, *298*, 126837; b) J. Du, T. D. Waite, P. M. Biesheuvel, W. Tang, *J. Hazard. Mater.* **2023**, *442*, 130023; c) Q. Xia, Q. Song, Z. Xu, *Waste Manage.* **2023**, *158*, 146–152.
[11] a) P. Rana, B. Kaushik, K. Solanki, K. M. Saini, R. K. Sharma, *Chem. Commun.* **2022**, *58*, 11354–11377; b) C. H. Mak, X. Han, M. Du, J.-J. Kai, K. F. Tsang, G. Jia, K.-C. Cheng, H.-H. Shen, H.-Y. Hsu, *J. Mater. Chem. A* **2021**, *9*, 4454–4504.
[12] H. Wang, Q. Tang, Z. Chen, T. Li, J. Wang, *Sci. China Mater.* **2020**, *63*, 2189–2205.
[13] a) A. Vinu, K. Z. Hossain, K. Ariga, *J. Nanosci. Nanotechnol.* **2005**, *5*, 347–371; b) F. Hoffmann, M. Cornelius, J. Morell, M. Fröba, *Angew. Chem. Int. Ed.* **2006**, *45*, 3216–3251; c) J. A. S. Costa, R. A. de Jesus, D. O. Santos, J. B. Neris, R. T. Figueiredo, C. M. Paranhos, *J. Environ. Chem. Eng.* **2021**, *9*, 105259; d) R. G. Acres, A. V. Ellis, J. Alvino, C. E. Lenahan, D. A. Khodakov, G. F. Metha, G. G. Andersson, *J. Phys. Chem. C* **2012**, *116*, 6289–6297; e) D. W. Kurka, M. Niehues, S. Kudruk, V. Gerke, B. J. Ravoo, *Chem. Eur. J.* **2021**, *27*, 7667–7676.
[14] I. A. Rahman, P. Vejayakumaran, C. S. Sipaut, J. Ismail, C. K. Chee, *Mater. Chem. Phys.* **2009**, *114*, 328–332.
[15] a) V. Kabanov, B. Heyne, *ACS Appl. Nano Mater.* **2020**, *3*, 8126–8137; b) O. Planas, N. Macia, M. Agut, S. Nonell, B. Heyne, *J. Am. Chem. Soc.* **2016**, *138*, 2762–2768; c) B. M. Estevão, F. Cucinotta, N. Hioka, M. Cossi, M. Argeri, G. Paul, L. Marchese, E. Gianotti, *Phys. Chem. Chem. Phys.* **2015**, *17*, 26804–26812; d) C. Mendoza, N. Emmanuel, C. A. Páez, L. Dreesen, J. C. M. Monbaliu, B. Heinrichs, *ChemPhotoChem* **2018**, *2*, 890–897; e) F. Ronzani, N. Costarramone, S. Blanc, A. K. Benabbou, M. Le Bechec, T. Pigot, M. Oelgemoeller, S. Lacombe, *J. Catal.* **2013**, *303*, 164–174; f) J. C. S. Terra, A. Desgranges, Z. Amara, A. Moores, *Catal. Today* **2023**, *407*, 52–58.
[16] a) S. Shanmugam, S. Xu, N. N. M. Adnan, C. Boyer, *Macromolecules* **2018**, *51*, 779–790; b) P. Li, G.-W. Wang, X. Zhu, L. Wang, *Tetrahedron* **2019**, *75*, 3448–3455.
[17] V. Kabanov, D. J. Press, R. P. S. Huynh, G. K. H. Shimizu, B. Heyne, *Chem. Commun.* **2018**, *54*, 6320–6323.
[18] a) J. C. S. Terra, A. Desgranges, C. Monnereau, E. H. Sanchez, J. A. De Toro, Z. Amara, A. Moores, *ACS Appl. Mater. Interfaces* **2020**, *12*, 24895–24904; b) G. J. Barbante, T. D. Ashton, E. H. Doeven, F. M. Pfeffer, D. J. D. Wilson, L. C. Henderson, P. S. Francis, *ChemCatChem* **2015**, *7*, 1655–1658; c) V. Blanchard, Z. Asbai, K. Cottet, G. Boissonnat, M. Port, Z. Amara, *Org. Process Res. Dev.* **2020**, *24*, 822–826; d) A. A. Yakushev, A. S. Abel, A. D. Averin, I. P. Beletskaya, A. V. Cheprakov, I. S. Ziankou, L. Bonneviot, A. Bessmertnykh-Lemeune, *Coord. Chem. Rev.* **2022**, *458*, 214331.
[19] a) K. Mori, M. Tottori, K. Watanabe, M. Che, H. Yamashita, *J. Phys. Chem. C* **2011**, *115*, 21358–21362; b) P. Rana, R. Gaur, B. Kaushik, S. Yadav, P. Yadav, P. Sharma, M. B. Gawande, R. K. Sharma, *J. Catal.* **2021**, *401*, 297–308.
[20] a) Y. Lin, M. Cai, Z. Fang, H. Zhao, *RSC Adv.* **2017**, *7*, 34722–34729; b) H. Zhao, W. He, R. Yao, M. Cai, *Adv. Synth. Catal.* **2014**, *356*, 3092–3098; c) Y. Lin, M. Cai, Z. Fang, H. Zhao, *RSC Adv.* **2016**, *6*, 85186–85193; d) F. Habeche, M. Hachemaoui, A. Mokhtar, K. Chikh, F. Benali, A. Mekki, F. Zaoui, Z. Cherifi, B. Boukoussa, *J. Inorg. Organomet. Polym. Mater.* **2020**, *30*, 4245–4268.
[21] R. Hosseinzadeh, N. Aghili, M. Mavvaji, *Polyhedron* **2022**, *213*, 115631.
[22] a) C. E. Housecroft, E. C. Constable, *Chem. Sci.* **2022**, *13*, 1225–1262; b) C. E. Housecroft, E. C. Constable, *Chem. Soc. Rev.* **2015**, *44*, 8386–8398; c) A. B. Muñoz-García, I. Benesperi, G. Boschloo, J. J. Concepcion, J. H. Delcamp, E. A. Gibson, G. J. Meyer, M. Pavone, H. Pettersson, A. Hagfeldt, M. Freitag, *Chem. Soc. Rev.* **2021**, *50*, 12450–12550.
[23] S. Sakaki, T. Kuroki, T. Hamada, *J. Chem. Soc. Dalton* **2002**, 840–842.
[24] F. J. Malzner, S. Y. Brauchli, E. Schönhofer, E. C. Constable, C. E. Housecroft, *Polyhedron* **2014**, *82*, 116–121.
[25] M. Karnahl, E. Mejía, N. Rockstroh, S. Tschierlei, S. P. Luo, K. Grabow, A. Kruth, V. Brüser, H. Junge, S. Lochbrunner, M. Beller, *ChemCatChem* **2014**, *6*, 82–86.
[26] I. Choi, V. Müller, G. Lole, R. Köhler, V. Karius, W. Viöl, C. Jooss, L. Ackermann, *Chem. Eur. J.* **2020**, *26*, 3509–3514.
[27] M. V. Appleby, P. G. Walker, D. Pritchard, S. van Meurs, C. M. Booth, C. Robertson, M. D. Ward, D. J. Kelly, J. A. Weinstein, *Materials Advances* **2020**, *1*, 3417–3427.
[28] a) I. K. Mbaraka, B. H. Shanks, *J. Am. Oil Chem. Soc.* **2006**, *83*, 79–91; b) C. G. Thomson, A.-L. Lee, F. Vilela, *Beilstein J. Org. Chem.* **2020**, *16*, 1495–1549; c) A. A. Kiss, A. C. Dimian, G. Rothenberg, *Adv. Synth. Catal.* **2006**, *348*, 75–81.
[29] W. Stöber, A. Fink, E. Bohn, *J. Colloid Interface Sci.* **1968**, *26*, 62–69.
[30] S. B. Yoon, J.-Y. Kim, J. H. Kim, Y. J. Park, K. R. Yoon, S.-K. Park, J.-S. Yu, *J. Mater. Chem.* **2007**, *17*, 1758–1761.
[31] a) P. Yadav, M. Yadav, R. Gaur, R. Gupta, G. Arora, P. Rana, A. Srivastava, R. K. Sharma, *ChemCatChem* **2020**, *12*, 2488–2496; b) R. Xiao, H. Zhao, M. Cai, *Tetrahedron* **2013**, *69*, 5444–5450.
[32] C. Li, R. Dickson, N. Rockstroh, J. Rabeah, D. B. Cordes, A. M. Z. Slawin, P. Hünemörder, A. Spannenberg, M. Bühl, E. Mejía, E. Zysman-Colman, P. C. J. Kamer, *Catal. Sci. Technol.* **2020**, *10*, 7745–7756.
[33] M. Ruthkosky, F. N. Castellano, G. J. Meyer, *Inorg. Chem.* **1996**, *35*, 6406–6412.
[34] D. Rehm, A. Weller, *Isr. J. Chem.* **1970**, *8*, 259–271.
[35] S.-M. Kuang, D. G. Cuttell, D. R. McMillin, P. E. Fanwick, R. A. Walton, *Inorg. Chem.* **2002**, *41*, 3313–3322.
[36] a) S. Cerfontaine, S. A. M. Wehlin, B. Elias, L. Troian-Gautier, *J. Am. Chem. Soc.* **2020**, *142*, 5549–5555; b) A. Soupart, F. Alary, J.-L. Heully, P. I. P. Elliott, I. M. Dixon, *Coord. Chem. Rev.* **2020**, *408*, 213184; c) R. Z. Boota, S. J. O. Hardman, G. P. Ashton, C. R. Rice, P. A. Scattergood, P. I. P. Elliott, *Inorg. Chem.* **2021**, *60*, 15768–15781; d) K. Eastham, P. A. Scattergood, D. Chu, R. Z. Boota, A. Soupart, F. Alary, I. M. Dixon, C. R. Rice, S. J. O. Hardman, P. I. P. Elliott, *Inorg. Chem.* **2022**, *61*, 19907–19924; e) J. K. White, R. H. Schmehl, C. Turro, *Inorg. Chim. Acta* **2017**, *454*, 7–20; f) S. Cerfontaine, L. Troian-Gautier, S. A. M. Wehlin, F. Loiseau, E. Cauët, B. Elias, *Dalton Trans.* **2020**, *49*, 8096–8106.
[37] C. A. Vincent, A. Ripak, L. Troian-Gautier, U. K. Tambar, *Tetrahedron* **2023**, *139*, 133364.
[38] T. Hering, D. P. Hari, B. König, *J. Org. Chem.* **2012**, *77*, 10347–10352.
[39] S. Fischer, D. Hollmann, S. Tschierlei, M. Karnahl, N. Rockstroh, E. Barsch, P. Schwarzbach, S.-P. Luo, H. Junge, M. Beller, S. Lochbrunner, R. Ludwig, A. Brückner, *ACS Catal.* **2014**, *4*, 1845–1849.
[40] Z. Singh, P. R. Donnarumma, M. B. Majewski, *Inorg. Chem.* **2020**, *59*, 12994–12999.
[41] J. Yuasa, M. Dan, T. Kawai, *Dalton Trans.* **2013**, *42*, 16096–16101.

Manuscript received: April 18, 2023
Accepted manuscript online: August 15, 2023
Version of record online: ■■, ■■

RESEARCH ARTICLE

Homoleptic and heteroleptic copper(I) complexes were anchored on silica nanoparticles and used for the visible-light mediated α-arylation of enol acetate.Photo-Catalyzed alpha-Arylation of Enol Acetate Using Recyclable Silica-Supported Heteroleptic and Homoleptic Copper(I) Photosensitizers (Troian-Gautier, Riant, Hermans et al.)

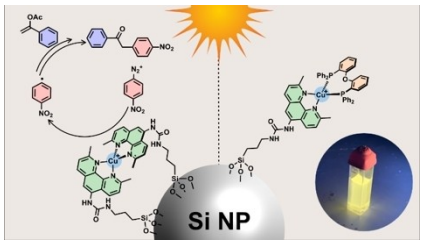

N. Body, Dr. R. Bevernaegie, Dr. C. Lefebvre, Prof. Dr. I. Jabin, Prof. Dr. S. Hermans, Prof. Dr. O. Riant*, Prof. Dr. L. Troian-Gautier**